NUTRIENT LIMITATION INCREASES CO_2-DEPENDENT SENSITIVITY OF C-ISOTOPIC FRACTIONATION IN *P. RETICULATUM*

By

Grace Dugdale

Utrecht University

Faculty of Geosciences

Department of Earth Sciences

March 2022

Supervised by:

Appy Sluijs

(Utrecht University)

Karen Brandenburg

(Utrecht University)

Universiteit Utrecht

NETHERLANDS INSTITUTE OF ECOLOGY (NIOO-KNAW)
NETHERLANDS INSTITUTE OF ECOLOGY (NIOO-KNAW)

Table of Contents

Figures

Tables

List of abbreviations

Abbreviation	*Explanation*
[…]	Concentration of "…"
ATP	Adenosine triphosphate
$\delta^{11}B$	Boron isotope composition
C	Carbon
^{12}C, ^{13}C	Stable carbon isotopes
CCM	Carbon concentrating mechanism
CO_2	Carbon dioxide
CO_2:O_2	Carboxylation: oxygenation
CO_3^{2-}	Carbonate ion
$\delta^{13}C_{CO_2}$	Isotopic composition of dissolved carbon dioxide
$\delta^{13}C_{DIC}$	Isotopic composition of dissolved inorganic carbon
$\delta^{13}C_{POC}$	Isotopic composition of particulate organic carbon formation
DIC	Dissolved inorganic carbon
ε_p	Stable isotopic fractionation of carbon
GS/GOGAT	Glutamine synthetase-Glutamate synthase
HAB	Harmful algal bloom
H_2CO_3	Carbonic acid
H_2SeO_3	Selenious acid
HCO_3^-	Bicarbonate ion
IRMS	Isotope ration mass spectrometry
LGM	Last Glacial Maximum
Lugol	Lugol's iodine solution
MeOH	Methanol
µ	Specific growth rate
N	Nitrogen
$NaH_2PO_4 \cdot 2H_2O$	Dihydrate sodium dihydrogen phosphate
$NaNO_3$	Sodium nitrate

N_0	Initial cell density
N_t	Cell density at time (t)
NPP	Net primary productivity
OA	Ocean acidification
P	Phosphate
PGA	Phosphoglyceric acid
pH_{NBS}	pH relative to the National Bureau of Standard buffers
pCO_2	Atmospheric CO_2
PETM	Palaeocene-Eocene Thermal Maximum
PO_4^{3-}	Phosphate ion
POC	Particulate organic carbon
PON	Particulate organic nitrogen
POP	Particulate organic phosphorus
RNA	Ribonucleic acid
RubisCO	Ribulose 1,5-bisphosphate carboxylase/oxygenase
SST	Sea surface temperature
TAC	Tricarboxylic acid cycle; Kreb's cycle; Citric acid cycle
VPDB	Vienna PeeDee Belemnite
YTX	Yessotoxin

Summary

Stable carbon isotope fractionation (ε_p) of marine phytoplankton is influenced by aqueous carbon dioxide concentrations ([$CO_{2(aq)}$]), cell morphology and metabolic pathways, which can further be influenced by environmental parameters, such as nutrient limitation. Increases in pCO_2 levels, and duo-limitation of nitrogen (N) and phosphorus (P) from strengthening of ocean stratification, are two of the predicted consequences of a changing climate due to anthropogenic fossil fuel consumption. In this study, we investigate *Protoceratum reticulatum,* an ecologically, economically and palaeo-environmentally significant yessotoxin-producing dinoflagellate, under representations of past (180 µatm), modern (400 µatm) and projected (1000 µatm) pCO_2 levels, in combination with limitation of essential nutrients N and P. Growth responses, internal stoichiometry, toxin production, and ε_p were all analysed for singular effects of nutrient and pCO_2, as well as the interaction between treatments. Toxin contents were independent of pCO_2 under nutrient replete treatments, but showed a negative correlation with pCO_2 under nutrient limitation. Highest toxin contents were found under nutrient limiting conditions at the lowest pCO_2 . Growth rates (µ) remained independent of nutrient limitation, and all growth response parameters (growth rate and population biovolume) were optimised around present day levels. PON and POP quota and production all decreased under nutrient limitation, and more so for the low CO_2 treatments. All nutrient ratios increased significantly with nutrient limitation, and caused deviations to the constant intracellular elemental stoichiometry that was otherwise maintained under nutrient replete treatments. POC quota and production, despite increasing under nutrient limtitation, maintained a constant relationship with stable carbon isotope fractionation for both nutrient treatments. ε_p remained strongly CO_2-dependent for both nutrient treatments, with significant increases in ε_p values observed under nutrient limitation. CO_2-dependent sensitivity of ε_p also increased under nutrient limitation, indicating potential changes in carbon species use and/or possible changes related to leakage. We found ε_p to be largely unaffected by µ, but largely influenced by POC content and pCO_2, and indirectly influenced by nutrient limitation, which could suggest changes in CCM mode or decrease in CCM functioning under nutrient limiting conditions. The potential increase in carbon fixation under nutrient limited conditions at high levels of pCO_2, in conjuction with increased intracellular carbon contents and changes in internal stoichiometry are likely to impact on oceanic carbon cycling of the biological pump, potentially altering the ocean's capacity to buffer carbon. The strong CO_2-dependency of ^{13}C fractionation, even at low pCO_2 levels, indicates a predominant diffusive uptake of CO_2 by *P. reticulatum* under both nutrient replete and nutrient limiting conditions. This, along with the increased CO_2-dependent sensitivity of ε_p under nutrient limiting conditions, provides potential for use of *P. reticulatum* in the running for a fossilized dinoflagellate CO_2 proxy. However, additional experiments should test for strain-specific inorganic carbon uptake mechanisms, as well as directly testing possible offsets that might occur for ^{13}C values between cells and cysts.

Introduction

Changing climate

Fluctuations of Earth's temperature over geological timescales coincides with natural variations in atmospheric CO_2 (pCO_2) (Hays et al. 1976; Ruddiman 2008). Over the past 800,000 years, variable pCO_2 values have stayed between 172 µatm – 300 µatm (Lüthi et al. 2008), with temperature anomalies remaining between -10 ˚C and 5˚C (with respect to mean temperature of the last millennium (Jouzel et al. 2007)). Since pre-industrial times, a rise in pCO_2 levels (Climate Change 2014 Synthesis Report IPCC 2014) from ~280 µatm to current levels of ~410 µatm (NOAA 2021). This rise in pCO_2, attributed to a substantial increase in anthropogenic fossil fuel consumption, is at least an order of magnitude faster seen for more than millions of years (Doney and Schimel 2007; Zalasiewicz et al. 2011), has already resulted in direct and indirect changes in the dynamic ocean climate on a decadal scale, such as increased sea-surface temperature (SST; IPCC 2019), decreased pH (Doney et al. 2009; IPCC 2019; Hurd et al. 2020), enhanced stratification (Yamaguchi and Suga 2019; Li et al. 2020), gyre expansion (Behrenfeld et al. 2006) and deoxygenation (Gruber 2011). By the end of the 21st century, models indicate pCO_2 levels to reach 1000 µatm if fossil fuel consumption is left unrestricted ('business-as-usual scenario of IPCC representative concentration pathway RCP8.5' (Meinshausen et al. 2011)). Therefore, it is of imperative importance to understand the underlying processes of ocean carbonate chemistry, to better understand how it might be affected by elevated pCO_2.

Direct consequences of pCO_2

The surface ocean carbonate system is directly impacted by changes in pCO_2, due to gaseous and substance exchange at the ocean surface and atmosphere interface. The direct diffusion of carbon dioxide (CO_2) into the ocean results in a rapid reaction with water, due to its high solubility, forming carbonic acid (H_2CO_3). This dissociates into the conjugated bases bicarbonate (HCO_3^-) and carbonate (CO_3^{2-}) ions , and protons (H+), of which the latter determines oceanic pH (Butler 1982). HCO_3^- is the most prevalent of the carbonate species at ~90%, followed by CO_3^{2-} (~9%), with only <1% remaining as $CO_{2(aq)}$ (**fig. 1**) (Zeebe and Wolf-Gladrow 2001; Middelburg 2019), which make up the total dissolved inorganic carbon (DIC; the sum of $CO_{2(aq)}$, HCO_3^- and CO_3^{2-}). The co-occurring equilibria reactions, along with the inability of HCO_3^- and CO_3^{2-} to be exchanged at the oceanic:atmospheric boundary and large volume of the ocean, has allowed the huge storage of anthropogenic pCO_2 (~24% cumulative total

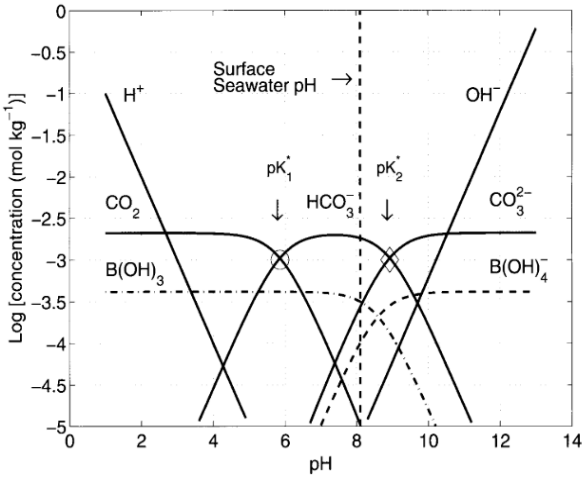

Figure 1 | The Bjerrum plot – concentrations of carbon species.
Concentrations of inorganic dissolved carbon species, at temperature 25C and 35 salinity (Zeebe and Wolf-Gladrow 2001). Dotted line indicates current surface seawater pH.

release of anthropogenic carbon (Friedlingstein et al. 2019)), and therefore highlights the ocean's crucial role in mitigating increases in pCO_2.

A rise in pCO_2 levels has already triggered increases in DIC and consequential shifts in marine carbonate speciation towards increased proportions of $CO_{2(aq)}$ and HCO_3^-, and a decrease in CO_3^{2-} and H+ (with a resultant drop in pH) (**fig. 1**). This acidifying of the ocean, known as 'ocean acidification' (OA) (Doney et al. 2009; Hallegraeff 2010; Gruber 2011; Middelburg 2019), is expected to intensify in the future (Caldeira and Wickett 2003). OA also has direct impact on marine organisms, such as a reduction in calcification and saturation level for calcifying species due to decreased pH and CO_3^{2-} (Doney et al. 2009) or an increase in carbon fixation by photo-synthesising organisms (Degens et al. 1968; Hinga et al. 1994; Hoins et al. 2015).

Indirect consequences of pCO_2

Anthropogenic greenhouse gas release has led to an increase in SST by ~0.7˚C over the last century (IPCC 2019), enhancing thermal and salinity gradient and therefore increasing the breadth and strength of stratification. Already observations have shown that 71% of the global increase in stratification between 1960-2018 was confined to the upper 200m, resulting predominantly (>90%) from temperature change (Li et al. 2020). A strengthening in stratification decreases mixing and transport between vertical layers in the ocean, therefore preventing gaseous and nutrient exchange between the upper and lower oceanic layers and altering light regimes. Already surface inorganic nitrogen (N) and phosphorus (P) concentrations are highly depleted in parts of the ocean, with N limitation or N and P co-limitation most commonly occurring (Zohary et al. 2005; Moore et al. 2008), the latter frequently seen in oligotrophic regions of the eastern Mediterranean (Tanaka et al. 2011), and the subtropical North Atlantic (Dyhrman et al. 2002; Lomas et al. 2004; Van Mooy et al. 2009). Increases in established stratified oligotrophic conditions impact on photosynthesising organisms predominantly living in the ocean surface layers, such as marine phytoplankton that predominantly rely on vertical mixing and nutrient influx from upwelling (Behrenfeld et al. 2006). Future predictions expect phytoplankton will experience rapid changes to the local oceanic climate, such as greater nutrient limitation, improved mixed-layer light and an extended growing season in the higher latitudes (Gittings et al. 2018).

Availability of key nutrient elements like C , N and P, can limit phytoplankton communities (Behrenfeld et al. 2006) through restricting production of essential compounds required for the functioning of key processes, such as photosynthesis, RNA-synthesis, ATP production, and protein and nucleic acid synthesis (Geider and La Roche 2002). Additionally, pathways of elemental acquisition can be coupled, so that limitation of one element can restrict processes or compounds necessary in the assimilation of another. One example is the C and N assimilation pathways, which are very closely coupled (Flynn 1991; Turpin 1991). Phosphoglyceric acid (PGA) assimilated from CO_2 supplies the tricarboxylic acid (TCA) cycle, producing 2-oxoglutarate as an intermediate metabolite. This compound is subsequently required for synthesis from inorganic N in the

glutamine synthetase/glutamate synthase (GS/GOGAT) cycle for amino acid metabolism (Dagenais-Bellefeuille and Morse 2013).

Biological activity of phytoplankton influences cycling of nutrients throughout the ocean, by both the depletion of nutrients (through nutrient uptake), and the enhancement of nutrient concentrations (via downward transport of organic material for remineralisation), also known as the 'biological pump'. Changes in nutrient availability can alter the elemental composition of phytoplankton, which can have subsequent impacts on the efficiency of the nutrient and carbon cycling of the ocean (Falkowski et al. 2000; Sigman and Boyle 2000). For example, high C:N ratios in particulate organic matter are expected to increase efficiency of the carbon and nitrogen pump, whereas higher C:P ratios could cause P limitation on nitrogen fixation. Photosynthesis from oceanic phytoplankton is thought to contribute roughly half of the biosphere's net primary productivity (NPP) (Field et al. 1998). However, during periods of enhanced upper ocean stratification, decreases in NPP have already been observed due to decreases in phytoplankton biomass resulting from nutrient limitation (Behrenfeld et al. 2006). Therefore, further increases in stratification are expected to have large impact on the ocean's nutrient and carbon cycling (Hallegraeff 2010).

Stable carbon isotope fractionation in phytoplankton

Carbon fixation within photosynthetic pathways discriminates against heavier stable carbon isotope (^{13}C) resulting in depletion of ^{13}C in the carbon isotopic composition ($\delta^{13}C$) of organic material relative to the carbon source. Early research indicating correlations between $\delta^{13}C$ of bulk sedimentary organic carbon and oceanic surface water [$CO_{2(aq)}$] (Sackett et al. 1965; Rau et al. 1989) provoked investigation towards the use of sedimentary organic $\delta^{13}C$ to estimate past oceanic and atmospheric CO_2 concentration changes (e.g. Sackett 1986; Jasper and Hayes 1990; Freeman and Hayes 1992; Bijl et al. 2010; Pagani 2014; Heureux and Rickaby 2015). Models of total carbon fixation using the flux of inorganic and organic carbon during C_3 synthesis of higher plants (Farquhar et al. 1982; Farquhar et al. 1989) provided the foundations for models of algal stable carbon isotopic fractionation (ε_p). Consequently, the most widely accepted ε_p model in phytoplankton can be calculated as the difference between the isotopic composition of extracellular CO_2 ($\delta^{13}C_{CO2}$) and particulate organic carbon ($\delta^{13}C_{POC}$) (Freeman and Hayes 1992). Many marine phytoplankton groups have exhibited sensitivity of ε_p to CO_2-availability, such as diatoms (Hinga et al. 1994; Laws et al. 1997; Hansen et al. 2007), coccolithophorids (Hinga et al. 1994; Rost et al. 2002) and dinoflagellates (Burkhardt *et al.*, 1999b; Hoins et al., 2015; 2016b; Wilkes *et al.*, 2017). However, some physiological traits have been identified to influence species' ^{13}C fractionation, includes growth rate (Pardue et al. 1976; Wong and Sackett 1978), cell size (Burkhardt et al. 1999a) and cell shape (Popp et al. 1998).

Yet, the primary forcing factor of CO_2-dependent fractionation in marine phytoplankton is thought to be the carboxylating enzyme in photosynthesis, RubisCO (Raven and Johnston 1991; Goericke et al. 1994). Most eukaryotes possess Form I RubisCO, except peridinin-containing dinoflagellates, which contain Form II (Morse et al. 1995) acquired by horizontal gene transfer from protobacterium (Whitney et al. 1995). The

mechanisms and extent of influence of Form II RubisCO on dinoflagellate ε_p expression remains an ongoing study area, due to intrinsic fractionating and catalytic properties. Despite dinoflagellate RubisCO able to distinguish between competing CO_2 and O_2 substrates (Lilley et al. 2010), it is continually debated whether C initially enters the cell as CO_2 and/or HCO_3^- (Rost et al. 2006a; Ratti et al. 2007; Brading et al. 2013) and its catalytic activity is difficult to measure due to rapid loss of activity after extraction from the cell. As HCO_3^- is enriched in ^{13}C relative to CO_2 (Mook et al. 1974), a greater proportion of HCO_3^- used in carbon fractionation results in a decrease of ε_p values. Observed rates of overall photosynthesis in dinoflagellates are not consistent with the low carboxylation:oxygenation (CO_2:O_2) specificity factor (Whitney and Andrews 1998), the low CO_2 affinity of RubisCO Form II (Badger et al. 1998), and the slow diffusion of $CO_{2(aq)}$ in water (more than 5,000 slower than air). Even at [$CO_{2(aq)}$] around triple current global mean of oceanic surface waters, the CO_2:O_2 ratio of dinoflagellate RubisCO was indicated at below a 50% energy loss level (Badger et al. 1998; Reinfelder 2011), which is significantly lower than for eukaryotes, such as diatoms and coccolithophores, containing form ID RubisCO (Badger et al. 1998; Whitney and Andrews 1998). One such way to compensate for the poor catalytic properties of RubisCO and ensure effective carboxylation is using carbon concentrating mechanisms (CCMs), which increase CO_2 concentration at the site of RubisCO (Giordano et al. 2005; Reinfelder 2011).

Current identified strategies of CCMs include the active uptake of CO_2 and HCO_3^-, the reduction of CO_2 leakage, and the use of carbonic anhydrase (CA), a ubiquitous enzyme that catalyses the dehydration of HCO_3^- to CO_2 (Giordano et al. 2005; Rost et al. 2006a; Reinfelder 2011), which may be intracellular (iCA) or extracellular (eCA). CCM activity in earlier evolved phytoplankton groups, such as dinoflagellates (Berner 2006), is thought greater than in later evolved phytoplankton groups (e.g. diatoms and haptophytes). Earlier evolved phytoplankton evolved during periods of higher CO_2 and lower O_2, therefore when pCO_2 levels decreased, effective CCMs were required for sufficient C uptake (Raven et al. 2008). Species-specific differences in CCM operation have been linked to differences in inorganic carbon acquisition (Giordano et al. 2005) which may subsequently alter and complicate the ε_p signal. Furthermore, other studies have indicated role of environmental conditions, such as light (Rost et al. 2002; Rost et al. 2006b; Hoins et al. 2016a) and nutrient availability (Hoins et al. 2016a), and not only do specifes-specific responses occur (e.g. Laws et al., 1995; Hoins et al., 2015; 2016b), but also strain-specific responses have been identified a dinoflagellate species, *Alexandrium ostenfeldii* (Brandenburg et al. 2021).

Dinoflagellates

Dinoflagellates are group of unicellular, predominantly marine and ecologically diverse phytoplankton (Burkholder *et al.* 2008; Lee *et al.*, 2016; Mitra *et al.*, 2016), with ecological significance attributed to the group's large contribution to primary productivity of coastal and shelf seas (Field et al. 1998; Behrenfeld et al. 2006). With shifts in resource availability and community dynamics due to climatic change, the motility and affinity of dinoflagellates to organic nutrient sources is likely competitive advantage in resource acquisition (Smayda and Reynolds 2003) especially in nutrient-limited environments (Smayda 1997), which

may potentially shift phytoplankton community dominance in their favour for the future (Klais et al. 2011; Klais et al. 2013).

Many species form blooms, which occur when chemical and physical factors (such as temperature, light and nutrients) favour growth processes over losses. Some high biomass blooms can be detrimental to ecosystems by inducing localised seawater deoxygenation (Black 2001), known as harmful algal blooms (HABs). Other HABs species can be harmful through production of toxins and bioactive compounds, which can have devastating ecological, commercial and economic impacts for the ecosystem, fisheries, health and tourism sectors e.g. (Peperzak 2003; Hernández-Becerril et al. 2007; Álvarez et al. 2011; Costa 2016; Sanseverino et al. 2016). For example, some toxins, such as yessotoxin (YTX), accumulate up the food web, causing illness and fatalities in marine life and fish. The consumption of seafood contaminated with HAB toxins can cause toxic syndromes in humans, such as paralytic shellfish poisoning (PSP) from saxitoxin, and be fatal in severe cases (Morquecho 2019). As such, the extent to which dinoflagellate HAB dynamics and physiology are affected by climate change consequences is an ongoing focus of huge importance (e.g. (Hallegraeff 2010; Moore et al. 2011; Wells and Karlson 2018; Brosnahan et al. 2020)). Primary factors thought to influence the degree of HAB durability and size are that affect growth response (Anderson et al. 2012), and external factors influencing toxin production, such as nutrient availability or pCO_2 levels. For example, many studies have linked toxicity increase to N limitation whereas for other species, such as *P. reticulatum*, an increase in YTX is seen under with severe P limitation, (Guerrini et al. 2007; Röder et al. 2012). Studies that investigate the response of toxin production to pCO_2 are of varied response. For example ,toxicity of *Karlodinium veneficum, A. ostenfeldii* and *A. catenella* increased with elevated pCO_2 (Fu et al. 2008; Kremp et al. 2012; Tatters et al. 2013), whereas decreases in toxicity have been observed in *A. fundyense* (Van De Waal et al. 2014).

Some HAB species may indicate species-specific traits that aid towards preventing mortality and encouraging species persistence, such as sexual resting cyst formation. Resting cysts are formed as part of the sexual cycle (Appendix I; SM: figure 18) and can be calcareous, siliceous, or organic-based material. They are often seen at the peak of a bloom or just preceding bloom termination (Wang et al. 2007; Choi et al. 2017), therefore thought likely triggered from nutrient limitation (Von Stosch 1973; Anderson and Lindquist 1985; Olli and Anderson 2002). Around 10% dinoflagellate species can produce a geologically preservable organic-walled resting cyst (Head 1996) which, due to their highly resistant macromolecular structures (e.g. Versteegh et al. 2007), can remain viable in marine sediment for up to 100 years (Ribeiro et al. 2011). Preceding this, the resilient dinoflagellate cyst ('dinocyst') shell can fossilize, and organic matter protected within the shell wall remains preserved in the sediment record. Dinoflagellates consist one of the richest group of protists in the fossil record, with fossilized dinocysts prevalent during the Mesozoic and Cenozoic (Fensome et al. 1996; Edwards 2012), and some found in sediments as old as the Triassic (~215 Ma BP) (Mantle *et al.*, 2020). Environmentally sensitive species often only have periodic appearances in the fossil record, whereas others, such as the early evolved organic dinocysts of *P. reticulatum* and *G. spinifera*

(Operculodinium centrocarpum and *Spiniferites ramosus* respectively), are ubiquitously recorded in marine sediments to the early Cenozoic (~65 Ma BP) and early Cretaceous (~144-99 Ma BP), respectively. Species-specific cyst morphological differences make them relatively easily identifiable, and consequently dinocysts have proven valuable biostratigraphic and palaeoenvironmental tools and proxies, such as palaeoindicators of sea surface temperature and productivity, salinity stratification and palaeo-oxygenation (De Vernal *et al.*, 1997; Pross and Brinkhuis, 2005; Sluijs *et al.*, 2005).

Reconstructing past CO_2 levels

Oceanic sedimentary strata records aspects of the past climate, such as sea surface temperature, marine bio-productivity, and ocean pH (Zalasiewicz and Williams 2009). Coupling these aspects with pCO_2 levels is imperative if reconstructions of past climate conditions aim to understand the effect of carbon cycling on the climate. However, direct measurements of pCO_2 from the atmosphere (Keeling 1960) and ice cores (Etheridge et al. 1998; Lüthi et al. 2008; Siegenthaler 2010; Petit et al. 2013) are time-limited to ~800,000 years BP. Reconstructions of earlier oceanic and climatic pCO_2 conditions typically require the use of proxies.

Current palaeo-CO_2 proxies employ a variety of techniques, such as stomatal indices in fossilized leaves (e.g. (Van Der Burgh *et al.*, 1993; Royer, 2001; Kürschner *et al.*, 2008)), boron isotope compositions ($\delta^{11}B$) in planktic foraminifera (e.g. (Pearson et al. 2009; Foster et al. 2012; Anagnostou et al. 2016; Hönisch et al. 2019)), and stable carbon isotopic ($\delta^{13}C$) fractionation of bulk sediments (e.g. (Freeman and Hayes 1990; Hayes et al. 1990; Raymo et al. 1996)) or algal remains (e.g. (Jasper and Hayes 1990; Freeman and Hayes 1992; Bijl et al. 2010; Pagani 2014; Witkowski et al. 2018)). Most proxies have limitations that stem from the proxy-specific processes that underly the generation, preservation, and analysis of signals, which can result in inaccuracies or bias. Proxies that use isotopic signatures can often vary in relation to the signal source for example, species-specific planktic differences in may bias $\delta^{11}B$ by using mixed and/or undetermined planktic species (Ni et al. 2007; Foster 2008), and bulk sedimentary $\delta^{13}C$ signals can vary with differences sediment composition (Glibert et al. 2019). Planktic isotopic proxies may also form bias through the processes and mechanisms involved in formulating the isotopic signal, for example species-specific CCMs in phytoplankton are likely the cause of discrepancies between the alkenone-based proxy and other proxies at low pCO_2 (Bolton and Stoll 2013; Stoll et al. 2019; Badger 2020). Nevertheless, old studies are continually revisited, and new studies performed, with the focus of reducing uncertainties, improving sensitivity, and increasing understanding the underlying mechanisms of signal formation that construct the palaeo-CO_2 estimates. For example, recent advances in technology have facilitated measurements as small as nanogram quantities of particulate organic carbon (van Roij et al. 2017), encouraging speculation for use of $\delta^{13}C$ in fossilized dinocysts as a novel species-specific proxy for palaeo pCO_2 (Hoins et al. 2015; Sluijs et al. 2018), which could potentially overcome uncertainty caused through species-specific physiological and metabolic differences.

As dinocyst formation of dinoflagellates at bloom termination is thought to be triggered by nutrient limitation (Olli and Anderson 2002; Wang et al. 2007), this indicates that $\delta^{13}C$ of dinocysts likely reflect the

conditions under which they were formed. However, for correct ascertainment, measurements of isotopic signals from the vegetative cell and cyst and quantifications between any isotopic relationship are imperative. Towards this aim, the following study investigates the response of ε_p to varying pCO_2 levels and nutrient availability for *P. reticulatum. P. reticulatum* is a bloom-forming and YTX-producing dinoflagellate (Satake et al. 1997; Eiki et al. 2005), which forms organic-walled resting cysts at bloom termination as part of its sexual reproductive cycle. The cyst of *P. reticulatum* (also referred to as *Operculodinium centrocarpum* sensu Wall and Dale (1966)) is the most cosmopolitan living cyst documented to date (Wall et al. 1977; Marret and Zonneveld 2003) with long biostratigraohic range (Head 1996), therefore providing considerable potential for both palaeo-environmental reconstruction and *in situ* studies.

Cultures will be grown under nutrient limitation and varying pCO_2 conditions to investigating species-specific responses related to carbon fixation, and the impact of the interaction of nutrient limitation and pCO_2 levels on the ε_p signal. Nutrient limited conditions are aimed to reconstruct conditions, such like at bloom termination, to promote cyst formation and enable comparisons between cells and cysts of the same culture. A sensitivity to turbulence has been previously documented for dinoflagellates (Thomas and Gibson 1990) with bubbles resulting from additionally gaseous input has been known to result in cell stress and mortality for some species (Berdalet et al. 2007; García Camacho et al. 2007), including *P. reticulatum* (Rodríguez et al. 2009), but pre-experimental trails (SM1 Pre-experiments), indicated VD5.2 strain of *P. reticulatum* able to maintain healthy populations with very gentle aeration. A closed culture system with continuous aeration of the media with pre-mixed pCO_2 will be used to minimalise fluctuations of $[CO_{2(aq)}]$, whilst allowing sufficient build-up of biomass for analysis of cells and cysts from the same replicate. Increases in pCO_2 levels are thought to reduce energy requirements for C assimilation, which could allow for reallocation of energy for growth and maintenance of nutrient stoichiometry. However, nutrient limitation is likely to reduce possible N and P assimilation, therefore likely resulting in increases to the internal elemental ratios. The increased C uptake with elevated pCO_2 is also therefore likely to increase relative nutrient stress on the cells under nutrient limiting conditions, which could increase cell toxicity (Guerrini et al. 2007; Röder et al. 2012). Increases in ^{13}C fractionation are likely at higher CO_2 availability, but relationships could deviate at lower pCO_2 levels for under nutrient replete conditions due to an increase in CCM activity. The N and P limitation could impact on formation of CCM functioning, therefore resulting in a higher dependency on diffusive uptake under nutrient limiting conditions, which is likely to be reflected in the cyst ε_p signal.

Materials and methods

Protoceratium reticulatum was exposed to nutrient replete or nutrient limited conditions under three different pCO_2 levels, with each treatment combination ran in triplicate. The nutrient replete treatments were terminated during the exponential phase (day 11), while nutrient limited treatments continued into the stationary phase, and ran for 42 days as we were interested in cyst formation.

Every 2-4 days samples for DIC, pH, temperature and cell counts were taken. At the end of each treatment samples for dissolved nutrients, particulate organic elements were also taken. How these parameters were determined is described below.

Species and experimental conditions

Stock cultures of *P. reticulatum* strain VD5.2 (isolated from Concarneau, France) were maintained at a constant temperature of 16°C in a nutrient replete growth medium. The nutrient replete treatment medium consisted of filtered and sterilized North Sea water (salinity of 36 psu), trace metals and vitamins added according to f/2 medium (Guillard and Ryther 1962), except for H_2SeO_3 which was added according to K medium (Keller et al. 1987).

The nutrient limited treatment medium was made with filtered sea water from the same source as used for the nutrient replete treatment medium (salinity of 36 psu). Vitamins and trace metals were added according to f/2 medium (Guillard and Ryther 1962), except for $NaH_2PO_4 \cdot 2H_2O$ and $NaNO_3$ which were each added to 5% volume (0.05 ml/L) of the nutrient replete medium to limit the carrying capacity to ~2000 cells/ml, and H_2SeO_3 which was added according to K medium (Keller et al. 1987).

From hereinafter treatments using the nutrient replete and nutrient limited media will be referred to as 'Replete' and 'Limited', respectively.

Prior to the experiment, Limited and Replete media were pre-aerated with air from pre-mixed gas bottles (Linde Gas Benelux, Dieren, the Netherlands), containing CO_2 concentrations of 180 µatm (representative of Last Glacial Maximum (Monnin et al. 2001)), 400 µatm (present day representation (Friedlingstein et al. 2020)) and 1000 µatm (representation of RCP8.5 2100 prediction (Meinshausen et al. 2011)). For ease of reading, the different CO_2 concentrations used in the treatments, will be referred to as the Low, Ambient and High (180 µatm, 400 µatm and 1000 µatm respectively) CO_2 treatments hereafter. The cultures of *P. reticulatum* were acclimated in airtight borosilicate 1L bottles containing the pre-aerated Limited/Replete medium to each pCO_2 treatment for 10 days (at least 5 generations).

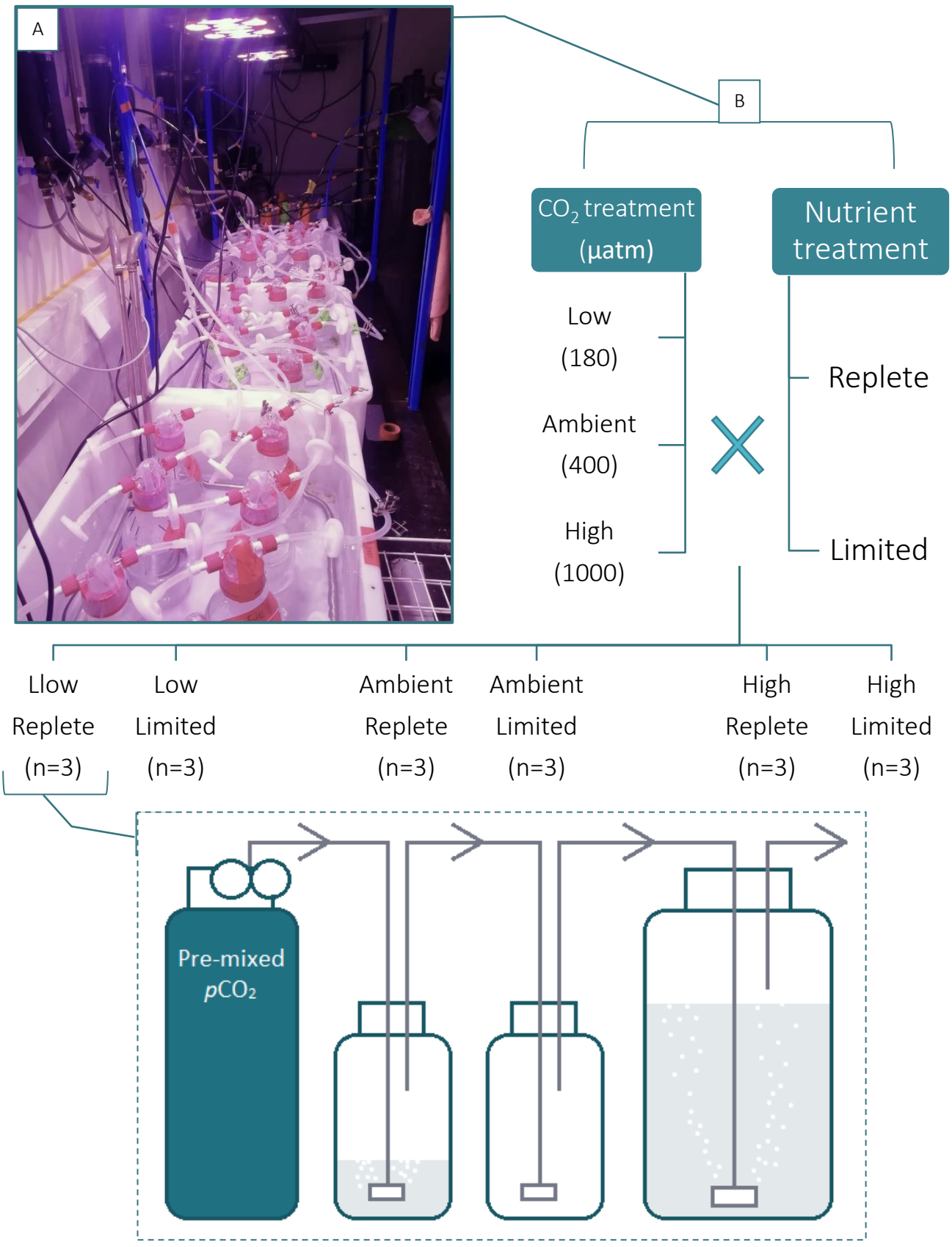

Figure 2 | Experimental set-up. (A) Photo of experimental set-up, with all treatments running in parallel. One water bath contains replicates (n=3) of both nutrient treatments for each CO_2 treatment, set at 16˚C.
(B) Schematic of treatment combinations (n=6), displaying interaction of CO_2 treatments (n=3; Low (180 µatm), Ambient (400 µatm), High (1000 µatm)) and nutrient treatments (n=2), with each treatment in triplicate.
(C) Schematic set-up of a single replicate, showing the flow of pCO_2 starting in the pre-mixed bottles, into 2 overflow bottles, to the replicate.

Throughout acclimation and the experiment, a continuous gas flow of the pre-mixed pCO_2 was input through a low flow rate of <0.1L/h (**fig. 2**). The continuous gaseous input allowed the maintenance of $[CO_{2(aq)}]$ at high dinoflagellate biomass – ensuring minimal changes in carbonate chemistry (Rost et al. 2008) – whilst providing homogeneous mixing within vessels without imposition on algal growth from turbulence (Thomas and Gibson 1990).

For the start of each treatment, cells from the acclimated cultures were transferred and grown in the experimental airtight borosilicate 1L bottles, with an initial density of ~70 cells mL^{-1}. Each combination of CO_2 treatment (Low, Ambient or High) X nutrient treatment (Limited or Replete) was run in triplicate (refer to **fig. 1B**), giving a total of 18 replicates (3 replicates for each treatment combination (n=6)). The resultant treatments were Low Replete, Low Limited, Ambient Replete, Ambient Limited, High Replete and High Limited. Temperatures were maintained at 16°C and cultures were exposed to a light:dark cycle of 16:8 h with daylight tubes. Mean irradiance was 77.25 µmol m^{-2} s^{-1} ± 27 µmol m^{-2} s^{-1}, and replicates were rotated at regular intervals to ensure an equal light exposure. Replete treatments were run for 11 days (at least 5 generations), and Limited treatments were run for at 42 days (at least 22 generations), after which cells were assessed for toxin content, elemental composition and ^{13}C fractionation.

Carbonate chemistry

pH and temperature measurements for Replete treatments were conducted every 2 days for the first half of the experiment, then daily in the second half. For Limited treatments, pH and temperature samples were conducted every 2 to 3 days until day 22, after which sampling was limited to every 3 to 4 days (see **SM: table. 7** for details of sample days). pH and temperature measurements were taken with a 2-point pH and temperature probe (inoLab pH7110, WTW, Weilheim, Germany). The probe was calibrated prior to each measurement to the National Bureau of Standards (NBS) scale. Samples for DIC analysis were taken simultaneous to pH and temperature measurements, stored at 4°C in the dark and without headspace. Concentration of DIC was done using a GasBench-II coupled to a Thermo Delta-V advantage isotope ratio mass spectrometer (precision of ±0.1‰).

Carbonate chemistry was calculated using CO2sys (Pierrot et al. 2006) using the pH_{NBS} and DIC measurements of each time point. Equilibrium constants (K_1 and K_2) of Mehrbach *et al.* (1973), refit by Dickson and Millero (1987), were used.

Size and population density

2mL samples were taken every other day, or every other day (dependent on growth rate), simultaneous to days of DIC samples and pH measurements, to determine cell population densities. Each sample was fixed with neutral Lugol's iodine solution (Lugol) to a final concentration of 1%, before storage in 4˚C in the dark until analysis, which was done with an inverted light microscope (DMI 4000B; Leica Microsystems CMS GmbH, Mannheim, Germany). For the final day of experiment, cell counts were done in triplicate to ensure accuracy and reliability of final counts.

Specific growth rates (μ) were calculated from cell counts and assessed for each replicate of each strain using the following equation:

$$N_t = N_0 \exp^{\mu t}; \qquad d^{-1}$$

where N_0 is the initial cell concentration, N_t is the cell concentration at time (t) and μ is the specific growth rate.

The 2mL samples of cells from each cell fraction from the final experimental day were fixed with Lugol to a final concentration of 1% and stored in 4˚C until analysis. Cell measurements (n=100 per replicate) were done with an inverted microscope (DMI 4000B; Leica Microsystems CMS GmbH, Mannheim, Germany) set to magnification of 200, and software Cell^D (Imaging software for Life Sciences Microscopy, Olympus, Tokyo, Japan). Cell diameters were used to calculate cell volume, assuming an oblate ellipsoid shape:

$$\text{volume} = \frac{4}{3}\pi a^2 b; \qquad \mu m^3$$

Where a = ½ measured cell width , b = ½ measured cell length

Population biovolumes were subsequently calculated by multiplying final population density with mean cell volumes.

Cell separation

For termination of the Limited treatments (t_{day} = 42) the CO_2 input was stopped for each replicate, whereby replicates were immediately induced with a light gradient (from the top to the bottom) and left for half an hour. Live cells were attracted towards the light (top of the bottle), while dead organic matter (DOM) and cysts remained on the container base. Cells were subsequently separated away from the cysts and DOM manually with a pipette. ~2mL samples were taken from each cell fraction for use in measurements of cell size and final density counts. The remainder of the cell fraction was used immediately for elemental and toxin analysis. As our experiments revealed negligible cyst formation, analysis was not viable or feasible. Therefore, the remaining methods are for the cell fraction only.

Elemental composition

Particulate organic carbon (POC), particulate organic nitrogen (PON) and particulate organic phosphorus (POP) were determined from ~20-40 mL culture material collected on pre-combusted glass microfibre filters (Whatman GF/F, Maidstone, UK). The filters were dried for 6 hours at 550˚C to eliminate any residual C and stored in the dark until used in the analyses.

For POC, PON and $\delta^{13}C_{POC}$ analyses, subsamples (~14%) of each filter were punched out and folded to fit into a tin cup. Samples were analysed in an elemental analyser (Flash 2000, Thermo Scientific, Karlsruhe, Germany) coupled to an isotope ratio mass spectrometer (IRMS, Thermo Scientific, Karlsruhe, Germany)

$\delta^{13}C_{POC}$ was reported relative to Vienna PeeDee Belemnite (VPDB) standard.

POP was analysed by combusting the remaining part of the filter (86%) for 30 min at 550˚C in Pyrex glass tubes, followed by digestion with 10mL persulfate for 30min at 120 ˚C. The digested solution was measured for PO_4^{3-} on a QuAAtro39 AutoAnalyser (SEAL Analytical Ltd., Southampton, UK).

Using calculations from (Burkhardt et al. 1999a), the elemental-specific growth rates were calculated. The carbon specific growth rate (POC production; pmol C $cell^{-1}$ day^{-1}), nitrogen specific growth rate (PON production; pmol N $cell^{-1}$ day^{-1}) and phosphorus specific growth rate (POP production; pmol P $cell^{-1}$ day^{-1}) were calculated through multiplication of µ and cellular elemental contents of POC quota (pmol C $cell^{-1}$), PON quota (pmol N $cell^{-1}$) or POP quota (pmol P $cell^{-1}$), respectively.

Toxicity measurements

At stationary phase of each replicate, ~10^5 cells were centrifuged to create algal pellets for quantification of intracellular yessotoxins. The algal pellet was transferred to 2mL microcentrifuge tubes before storage at -20˚C until analysis. Samples were analysed according to the protocol set at Ifremer, LER-BO.

Mixer Ball Milling equipment (Mixer Mill MM400, Retsch) was used to extract Yessotoxin (YTX) and homo-Yessotoxin (h-YTX) from cells. 400µl of Methanol and glass beads (150 mg, 100–250 µm in diameter) were added to the cell pellets. Samples were shaken at 30 Hz for 30 minutes with MM400 equipment. After centrifugation at 15000 g, the supernatant was transferred into a 1.5 mL Eppendorf tube. The cells pellets were re-extracted twice by 400 µl and 200 µl of Methanol and shaking at 30 Hz for 30 minutes. The supernatants were pooled. 200 µl of methanolic extract was ultrafiltered (0.20 µm, Nanosep MF, Pall) and transferred into an HPLC vial before LC-MS/MS analysis.

Samples analyses were performed by LC-MS/MS using a Shimadzu UFLCxr system coupled to a triple quadruple hybrid mass spectrometer Q-Trap (API400QTrap, Sciex) equipped with a heated electrospray ionization (ESI) source. Data acquisitions were performed using negative ion mode and MRM (Multiple Reaction Monitoring) mode. Chromatographic separation was carried out on a reversed-phase column Xbridge BEH C18 (50 x 2.1 mm, 2.5 µm, Waters) equipped with a guard column (5 x 2.1 mm, 2.5 µm, same stationary phase as column). Water (A) and acetonitrile 90% (B) both containing 6.7 mM of ammonium hydroxide were used as mobile phases at a flow rate of 400 $\mu l.min^{-1}$. The following gradient was used: 0 min, 5% B; 1.50 min, 5% B; 4.5 min, 65% B; 5.00 min, 100% B; 7.00 min, 100% B; 7.50 min, 5% B; 12.00 min, 5% B. The oven temperature was 30°C and the injection volume was 5 µL. The ESI interface operated using the following parameters: curtain gas 20 psi, temperature: 600 °C, gas1 60 psi; 08/04/2020 A. Derrien 2/6 gas2 60 psi, ion spray voltage -4500 V. The transitions and MS/MS parameters are presented in Table 2. Quantification was performed relative to the YTX and h-YTX standards (National Research Council Canada, NRCC) with a 6-point calibration curve. The limit of quantification was 0.03 ng mL^{-1}.

Table 1 | Precursor ions, product ions and MS/MS parameter used for the detection of YTX and h-YTX

Toxins	Q1 (M/Z) $[M-2H]^{2-}$	Q3 (M/Z)	Collision Energy (CE) (EV)	Cell Exit Potential (CXP) (V)	Dwell Time (DT) (MS)
YTX	570.4	396.4	-46	-9	130
	570.4	467.4	-42	-11	130
H-YTX	577.2	403.4	-46	-9	130
	577.2	474.4	-42	-11	130

Isotopic fractionation

The isotopic composition of the dissolved inorganic carbon ($\delta^{13}C_{DIC}$) was measured simultaneous to measurements of DIC concentration, using a GasBench-II coupled to a Thermo Delta-V advantage isotope ratio mass spectrometer (precision of ±0.1‰).

A mass balance relation from Zeebe and Wolf-Gladrow (2001) was used to convert the measured $\delta^{13}C_{DIC}$ to the isotopic composition of dissolved CO_2 in the water ($\delta^{13}C_{CO_2}$). The stable carbon isotopic fractionation during particulate organic matter build-up (ε_p) was subsequently calculated using a relationship found by Freeman and Hayes (1992). Means of the final 6 sample days of carbonate parameters were used in the calculations of ε_p to better represent DIC concentrations that cells were exposed to and reduce error from natural fluctuations.

$$\varepsilon_p = \frac{(\delta^{13}C_{CO_2} - \delta^{13}C_{POC})}{(1+\frac{\delta^{13}C_{POC}}{1000})}$$

Temperature-dependent fractionation factors between HCO_3^- and CO_3^-, and CO_2 and HCO_3^-, were applied and calculated according to Zhang *et al.* (1995) and Mook *et al.* (1974).

Statistical analyses

Statistical analyses were performed in RStudio version 1.2.5033 (R Development Core Team 2019). Linear regressions were used to determine the correlation between the tested variables to both fixed effects and interactive effects of nutrient treatments and CO_2 treatments to assess significant responses. Data was checked for normality and residuals were checked for heteroscedasticity. Pairwise comparisons were done using the Tukey method.

Results

Experimental treatments

Within nutrient treatments, carbonate chemistry parameters remained different between CO_2 treatments (**table. 2**; $P<0.001$ for all), except DIC which did not differ between the Limited treatments (**table. 2**). pH, pCO_2 and $[CO_{2(aq)}]$ did not differ between nutrient treatments of the Low or High treatment, however, Ambient treatments did ($P=0.01$) in conjunction with a large build up in biomass (**SM: fig. 13, 14**). Mean pCO_2 of the Low treatments ranged between 110 and 153 µatm, between 215 and 300 µatm for the Ambient treatments, and between 688 and 698 µatm for the High treatments.

Table 2 | Overview of carbonate chemistry parameters in the treatments are indicated as triplicate means of the final 6 sample days and standard deviation of the mean (sd) for each treatment (n=6). Significant differences between treatments are indicated by superscript letters ($P<0.05$).

Nutrient regime	CO_2 treatment	pH		DIC (µmol L^{-1})		pCO_2 (µatm)		$[CO_{2(aq)}]$ (µmol L^{-1})	
		mean	*sd*	*mean*	*sd*	*mean*	*sd*	*mean*	*sd*
Replete	Low	8.527 ^{a}	0.03	1959 ^{a}	18.97	110.0 ^{a}	12.79	**3.58** ^{a}	**0.40**
	Ambient	8.313 ^{b}	0.06	2149 ^{c}	18.27	215.2 ^{b}	39.40	**6.93** ^{b}	**1.25**
	High	7.860 ^{c}	0.03	2317 ^{d}	44.59	697.8 ^{c}	42.47	**22.83** ^{c}	**1.24**
Limited	Low	8.407 ^{d}	0.006	2071 ^{b}	40.61	153.9 ^{a}	3.03	**5.06** ^{a}	**0.12**
	Ambient	8.143 ^{e}	0.02	2012 ^{b}	38.67	299.6 ^{d}	4.72	**9.66** ^{d}	**0.08**
	High	7.823 ^{c}	0.006	2092 ^{b}	42.00	687.9 ^{c}	11.24	**22.44** ^{c}	**0.41**

Initial dissolved N and P concentrations for Replete treatments were 3.98 ± 0.86 mg N L^{-1} and 0.34 ± 0.03 mg P L^{-1} respectively (**fig. 3**). For Limited treatments Initial dissolved inorganic N (DIN) and P (DIP) concentrations were 0.89 ± 0.25 mg N L^{-1} and 0.06 ± 0.02 mg P L^{-1}, respectively. DIP and DIN concentrations reached depletion in the Limited treatments for all treatments whereas dissolved nutrients remained in abundant supply for cells under Replete treatments, and never became limiting (**fig. 3**).

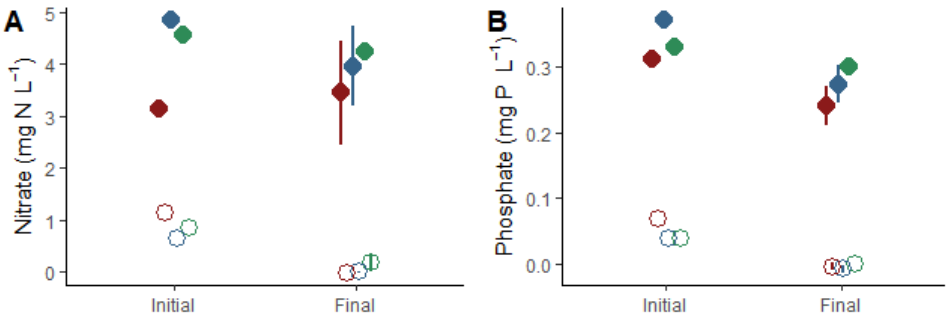

Figure 3 | Dissolved (A) nitrate and (B) phosphate concentrations at the beginning and end of experiment. Where triplicate means for each treatment (n=6) are represented by circles, and error bars indicate standard deviation of the mean. Nutrient treatment is indicated by filled (Replete) or hollow (Limited) circles, and colours represent CO_2 treatments (Low = green; Ambient = blue; High = red). Circles are staggered slightly horizontally for visual purposes only, and do not affect actual values of dissolved nutrients.

Population densities and growth

Initial population densities for all replicates were 70 cells ml^{-1} ± 8 cells mL^{-1} (**SM: fig. 12.**). All treatments entered an initial exponential growth phase, during which final population densities for the Replete treatments were taken ($t_{replete,\ final}$ = 11 days). Population densities in Replete treatments were consistently significantly larger than in Limited treatments (*P*<0.001), with the Ambient Replete treatment displaying the highest final population density (**SM: fig. 12**) of 5389 ± 625 cells mL^{-1}. Final population densities in the High and Low treatments were 4461 ± 953 cells mL^{-1} and 3540 ± 263 cells mL^{-1}, respectively.

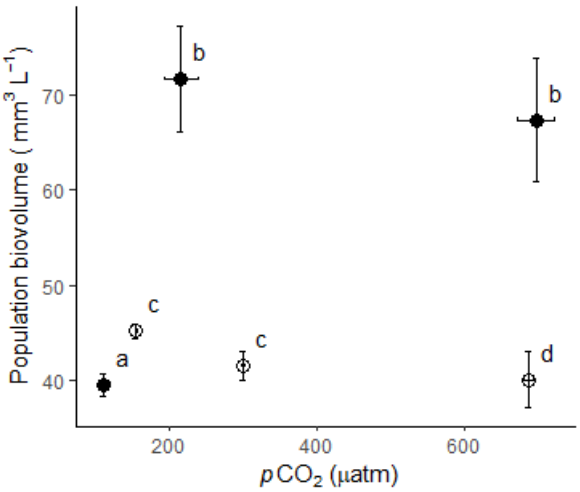

Figure 4 | Final population biovolumes of treatments against final pCO_2 levels of treatments. Solid circles indicate Replete treatments, and hollow circles indicate Limited treatments. Error bars indicate standard deviation of triplicate means. Lowercase letters indicate relationships of significance.

Limited treatments reached a population threshold/stationary phase (at 8 days for the Ambient and High treatments, and 10 days for Low treatment), after which population densities remained stable (**SM: fig. 12**) for the duration of the experiment. The Low treatment exhibited the greatest final population density of 2419 ± 89 cells mL^{-1} for the Limited treatments (**table. 3**). The Ambient and High Limited treatments had final population densities of 2101 ± 56 cells mL^{-1} and 1622 ± 131 cells mL^{-1} respectively (**table. 3**).

Cell volumes increased as a function of pCO_2 (*P*<0.001), with the largest volumes observed in the High CO_2 treatment. Cell volumes also significantly increased under nutrient limitation(*P*<0.001; **table 3**), with the greatest cell volumes therefore observed under High Limited treatments. Detailed measurements of cell width and length are given in **SM**: **table. 8.**

Table 3 | Growth response, elemental ratios and ε_p values. Mean values (n=3) and standard deviation (sd) are given for population densities (count mL^{-1}), cell volume (um^3), µ (d^{-1}) and ε_p (‰). Significant differences between treatments are indicated in the table by superscript letters (following values) (*P*<0.05).

Nutrient regime	CO_2 treatment	Population density (count mL^{-1})		Cell volume (um^3)		µ (d^{-1})		**ε_p** (‰)	
		mean	*sd*	*mean*	*sd*	*mean*	*sd*	*mean*	*sd*
Replete	Low	3540 ^{a}	263	11222^{a}	1114	0.38 ^{a}	0.01	7.85 ^{a}	0.31
	Ambient	5289 ^{b}	625	13558^{b}	724	0.42 ^{b}	0.004	8.58 ^{a}	0.87
	High	4461 $^{a, b}$	953	15238^{c}	997	0.38 ^{a}	0.01	10.11^{a}	0.51
Limited	Low	2419 ^{c}	89	18715^{d}	1220	0.37 ^{a}	0.01	10.06^{a}	1.53
	Ambient	2101 $^{c, d}$	56	19756^{d}	1141	0.44 ^{b}	0.02	12.56^{b}	0.67
	High	1622 ^{d}	131	24702^{e}	2207	0.40 ^{a}	0.01	16.92^{c}	0.56

Population biovolumes of the Replete treatment exhibited the largest range (38.19 mm^3 L^{-1} to 82.90 mm^3 L^{-1}; **fig. 4**), where maximum biovolumes were observed in the Ambient treatment (71.73 ± 9.68 mm^3 L^{-1}). In comparison, Limited treatments (ranging from 37.03 mm^3 L^{-1} to 46.62 mm^3 L^{-1}) exhibited a slight inverse correlation with pCO_2, with the lowest biovolumes observed in the High treatment (P<0.05). Replete Ambient and High treatments were significantly greater than Limited treatments (P<0.05 and P<0.001, respectively), whereas biovolumes of the Low Replete treatment were significantly lower than the Low Limited treatment (P<0.001).

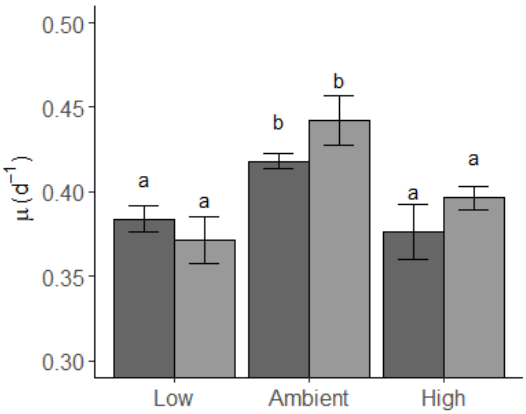

Figure 5 | Specific growth rate of *P. reticulatum* in each treatment. Dark grey represents nutrient replete treatments, light grey represents nutrient limited treatments. Significant differences are shown by lowercase letters. Error bars indicate standard deviation.

Specific growth rates (μ) (0.36 d^{-1} to 0.45 d^{-1}) were independent of nutrient limitation (**fig. 5, table 3**), but dependent on CO_2 treatment. μ in both Ambient treatments (0.43 ± 0.02 d^{-1}) was ~12.5% higher than μ in Low (0.38 ± 0.01 d^{-1}; P<0.001) or High (0.39 ± 0.02 d^{-1}; P<0.001) treatments.

Nutrient production and elemental stoichiometry

The nutrient ratios of C:N, N:P and C:P under Replete treatments were independent of pCO_2 (7.58 ± 0.34, 12.05 ± 0.82 and 91.18 ± 4.96, respectively). Within Limited treatments, C:P ratios also remained constant (462.77 ± 50.15), whereas ratios in the Low treatment deviated from the two higher CO_2 treatments (**fig. 6 A, B**) for C:N (>30% increase; P<0.001) and N:P (>35% decrease, P<0.05).

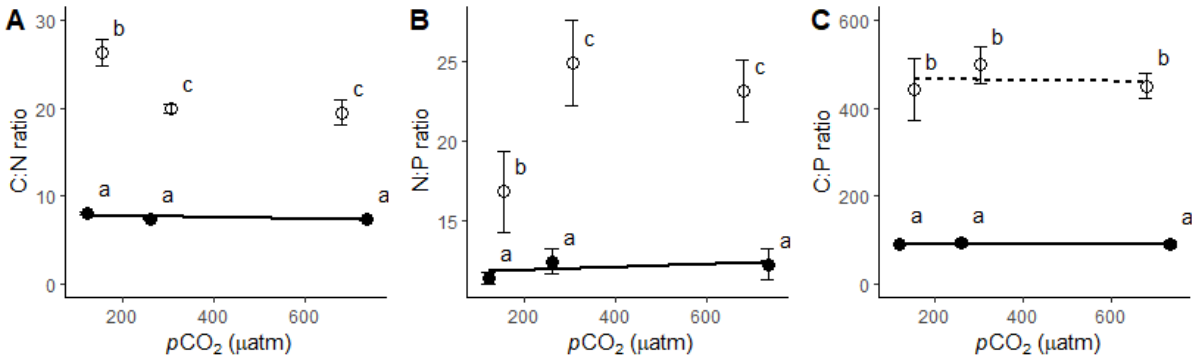

Figure 6 | Cellular nutrient ratios as a function of pCO_2. Circles represent mean (n=3) of Replete (solid) and Limited (hollow) replicates for each CO_2 treatment with error bars representing standard deviation. Significant linear regression (P<0.05) is indicated with solid (Replete) or dashed (Limited) lines, and differences between treatments with different lower-case letters.

All nutrient ratios were significantly larger (P<0.001) in Limited treatments as compared to Replete treatments (**fig. 6**). This increase in ratios was reflected within the intercellular element quotas (**fig. 7 A, B, C**). Nutrient limitation significantly increased POC quota for all CO_2 treatments (P<0.001), which was over two-fold for Ambient and High treatments. Additionally, Limited treatments displayed significantly reduced POP quota (P<0.001) to almost half of values seen in replete nutrient conditions. PON quotas in Limited treatments were lower than Replete treatments, but a signficance in difference was only found under Low CO_2 conditions (P<0.005).

Elemental quotas and μ were combined to indicate POC, PON and POP production (**fig. 7 D, E, F**). Low treatments for both Replete and Limited treatments resulted in lower values of POC, PON and POP production as compared to Ambient or High treatments. Within the Limited treatments, these lower values in the Low treatment were all significant (POC production, P<0.05; PON production, P<0.005; POP production, P<0.001). Whereas, only PON and POP production were significantly lower at the Low Replete treatment. Between nutrient treatments, POC production displayed greater values in the Limited treatments (P<0.001), whereas POP production (P<0.001) was significantly decreased in the Limited treatment. PON production is also decreased under Limited treatments as compared to Replete treatments, yet this difference was not significant related to the relatively small changes between nutrient treatments of the Ambient and High treatments.

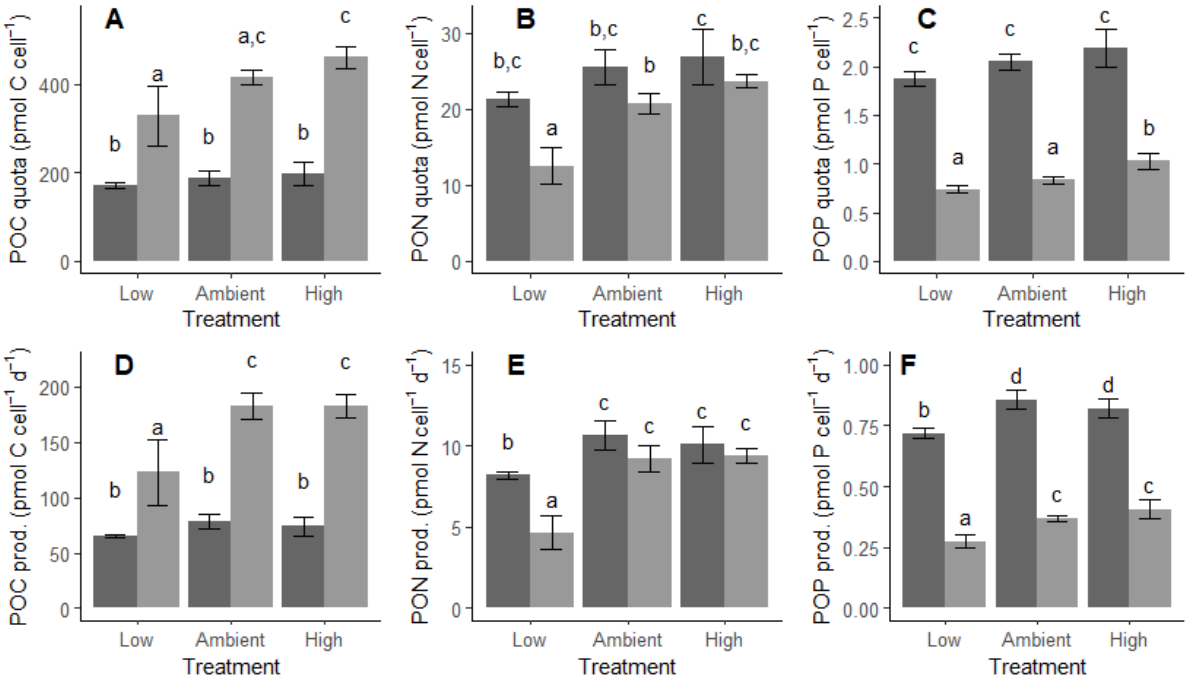

Figure 7 | Nutrient content (A, B, C) and production (D, E, F) of *P. reticulatum* grown under different CO_2 treatments and Replete (dark grey) or Limited (light grey) nutrient treatments. Error bars represent standard deviation of the triplicate mean and lowercase letters indicate significant statistical difference (P<0.05).

Carbon isotopic fractionation

ε_p values observed in Limited treatments ranged from 8.64‰ to 17.56‰, and were significantly greater (P<0.005) than ε_p values in Replete treatments (7.65‰ to 10.42‰). POC quota and POC production both positively correlated with ε_p (R^2 = 0.68, P<0.001 and R^2 = 0.64, P<0.001 respectively) and remained independent of nutrient treatment (**fig. 8 A, B**), where higher ε_p values were seen with greater POC quota and POC production. Strong positive correlations occured between ε_p and $[CO_{2(aq)}]$ for both Replete (R^2 = 0.78, P<0.005) and Limited (R^2 = 0.9, P<0.001) treatments, with greater ε_p values at higher $[CO_{2(aq)}]$ (**fig. 8 C**). Stronger increases of ε_p to increasing $[CO_{2(aq)}]$ were observed under Limited treatments than Replete treatments (**fig. 8 C**), indicating a greater sensitivity of ε_p to changes in $[CO_{2(aq)}]$ under limiting nutrient conditions.

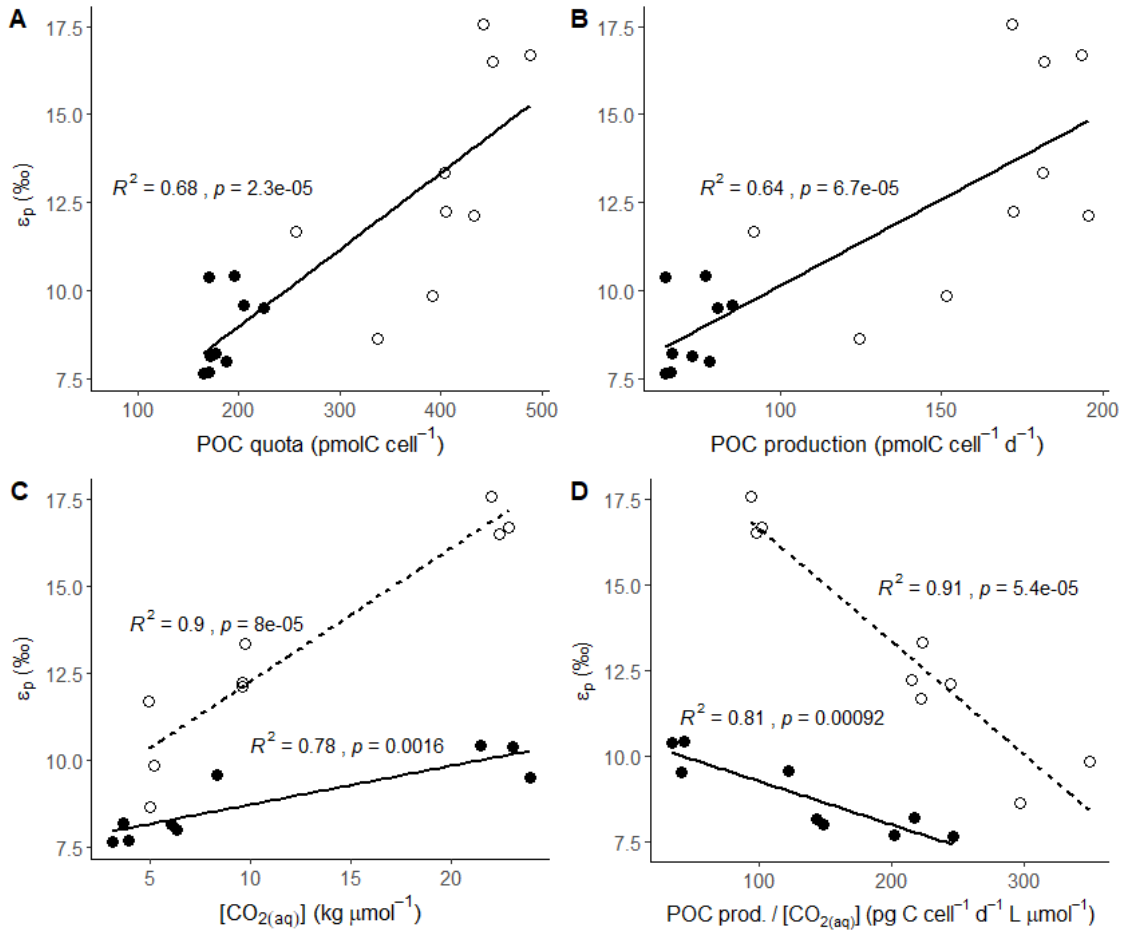

Figure 8 | ε_p as a function of (A) POC quota, (B) POC production (C) $[CO_{2(aq)}]$ and (D) POC production/$[CO_{2(aq)}]$ for *P. reticulatum*. Circles represent replete (solid) and nutrient limited (hollow) replicates for each CO_2 treatment (n=3). Linear correlations with relationships where *P<0.05* are shown. For (C) and (D), the dashed and solid lines indicate the limited and replete treatments respectively.

When corrected for C demand, ε_p exhibited a strong negative linear relationship with POC prod/$[CO_{2(aq)}]$ (i.e. C demand over supply) for both Replete (R^2 = 81, P<0.005) and Limited treatments (R^2 = 0.91, P<0.005) (**fig. 8D**), where Low treatments had a lower C supply compared with demand and High treatments had a

relatively low C demand compared to supply. Nutrient limitation resulted in a larger C demand/supply as compared to Replete treatments, correlating with increases in POC production (**fig. 7D**).

Cellular toxicity

The repeatability of the YTX results is good, except for two values that appear to be outliers (**fig. 9 A**). Further analysis of the samples was done to check the efficiency of extration and dilution, but no anomalies were detected during analysis and no evidence was found to explain the poor repeatability. Therefore, the outliers have been disregarded in further analysis.

Very high concentrations of Yessotoxin (YTX) were found compared to homo Yessotoxin (h-YTX) (**fig.9 A, B**), making up >99.9% all YTXs in every replicate. YTX values in the Limited treatments range from 4626 ± 1398 fg YTX cell^{-1} (High) to 24452 ± 980 fg YTX cell^{-1} (Low). h-YTX concentrations in the Limited treatments range from 0.49 ± 0.03 fg YTX cell^{-1} (Ambient) to 0.89 ± 0.04 fg YTX cell^{-1} (Low), and are significantly greater than h-YTX concentration in Replete treatments (P<0.001). All hYTX contents for each CO_2 treatment increased under nutrient limiting conditions (P<0.001). In comparison, YTX content did not differ between Ambient Replete and Limited treatments, but increased with nutrient limitation for the Low treatments (P<0.001) and decreased with nutrient limitation in the High treatments (P<0.001).

Both YTX and h-YTX concentrations in Replete treatments are independent of changes in pCO_2. In comparison, a dependency of YTX content on pCO_2 was observed under nutrient limiting conditions, where YTX decreased with increasing pCO_2 at highest YTX content of 24.45 ± 0.98 pg YTX cell^{-1} in the Low Limited treatment and lowest YTX content (4.63 ± 1.40 pg YTX cell^{-1}) in the High Limited treatment.

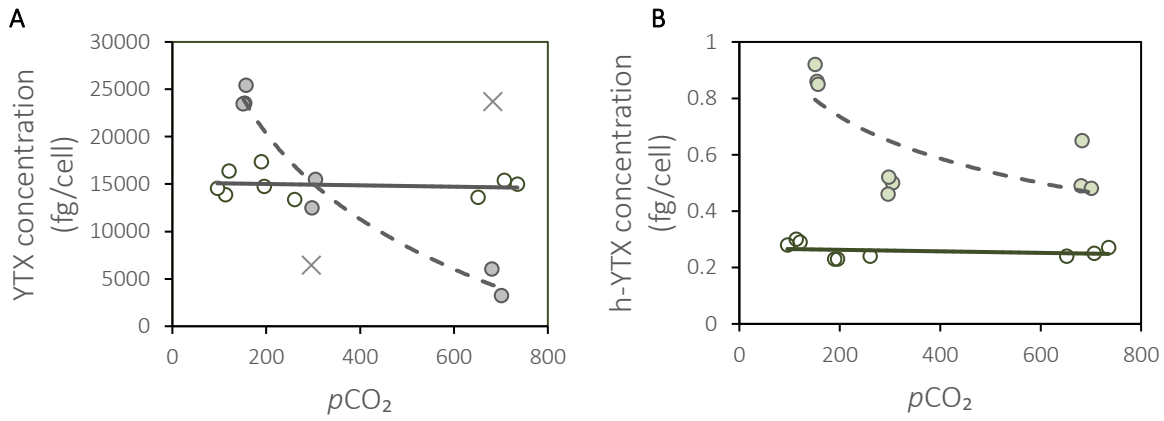

Figure 9 | Concentration of Yessotoxin (A) and homo-Yessotoxin (B) production in samples, compared with treatment pCO_2. Where replete nutrient treatments are indicated by hollow circles and solid best fit lines, and limited nutrient treatments are indicated with filled circles and dashed best fit lines. The two crosses (A) indicate two outliers from limited treatments that resulted in an abnormally large coefficient of variation (40.3% and 101.0% for Ambient and High treatments only) if included. Therefore, these two results are left out when calculating the best fit line.

Discussion

In this study we investigated ^{13}C fractionation of *P. reticulatum* over 6 different treatments, with varying pCO_2 levels (Low, Ambient and High) and nutrient availabilities (Replete and Limited). ^{13}C fractionation increased linearly with increasing pCO_2 for both Replete and Limited treatments, with an increase in CO_2-dependent sensitivity under Limited treatments. As ^{13}C fractionation could relate to changing growth parameters, we investigated growth rates, POC quota and POC production for each treatment. POC quota and POC production increased under nutrient limitation. While POC quota and POC production were unaltered over the pCO_2 range in Replete treatments, they were lower in the Low Limited treatments relative to the two higher CO_2 treatments. Highest CO_2-dependent sensitivities were observed at the combination of low carbon demand (low POC quota and production) with high carbon supply (High CO_2 treatments). As growth parameters might be affected by the intercellular elemental stoichiometry, PON and POP quota and production and elemental ratios (C:N, C:P and N:P) were investigated. Nutrient limitation resulted in decreases in PON and POP quota and production, and all nutrient ratios increased. Toxin content in Replete treatments remained unaltered by changes in CO_2 availability but decreased with increasing pCO_2 under nutrient limiting conditions.

Experimental set-up

Despite the constant aeration of media, some pH drift was observed, especially for the Ambient treatment (**table. 2:** compare pCO_2 with CO_2 treatment), due to the large biomass build-up (**fig. 4**). Changes in carbonate chemistry from high dinoflagellate cell densities naturally occur when rates of inorganic carbon consumption (due to increased photosynthesis) outweigh the rate at which the inorganic carbon pool is replenished (largely due to the relatively slow diffusivity of CO_2 in water). This is commonly seen in nature resulting from bloom formation specifically when large biomasses are formed (Hansen 2002; Brandenburg et al. 2017). To minimize carbonate chemistry fluctuations, some previous studies have limited maximum cell densities (Hoins *et al.*, 2015; Hoins *et al.*, 2016; Hoins *et al.*, 2016) which can limit the applicability (in some cases) of experiments. For example, constraining phytoplankton population densities to <400 cells mL^{-1} for blooming characteristics of species that naturally bloom in higher densities would be unrealistic, such as *Gonyaulax spinifera* (Rhodes et al. 2006) which is documented to densities of 2-3 x 10^6 cells L^{-1} (Ingarao et al. 2006), or *Scrippsiella trochoidea* which can reach >30 000 cells mL^{-1} (Wang et al. 2007). Under such high densities, light might be limiting due to self-shading (REF) or local nutrient resources could be more rapidly depleted than if under lower concentrations, which could form bias in analyses of internal stoichiometry or photosynthesising processes. However, it must remain under consideration that *P. reticulatum* frequently has peak bloom densities of <400 cells mL^{-1} in nature (Koike et al. 2006; Rossi and Fiorillo 2010; Álvarez et al. 2011). This experiment was designed to enable sufficient biomass for statistically viable measurements of many parameters for both cyst and cell analysis, however we cannot overlook the fact that cell densities reached concentrations greater than if found in nature.

Both N and P were depleted to low/ undetectable concentrations in the Limited growth media (**fig. 3**). The point at which nutrients began to limit growth is insinuated from the plateau in population densities (**SM: fig. 12**). This plateau and stabilisation implies an absence of cell division (rather than cell mortality), indicating P-limitation over N-limitation for the primary limiting nutrient as P is necessary for RNA synthesis (Li et al. 2016). Primary nutrient limitation by P was also confirmed by the relatively large decrease in POP quota and production with nutrient limitation (**fig 7 C, F**), and increase in C:P and N:P (**fig. 6**)). At cell cycle arrest, dinoflagellates generally either form cysts (Wang et al. 2007), or continue photosynthesising and store internal metabolites, such as C, N and P (Dortch et al. 1984), until the limiting nutrient becomes readily available again (Lei and Lu 2011; Li et al. 2016). Some cysts were formed for the duration of this experiment albeit not enough for analysis, despite indicating significant formation during preliminary experiments (**SM1 Preliminary experiments**) and the acclimation period. One reason for this could be the acclimatising of cells to the nutrient limited media during the acclimation, therefore not providing enough stress for cyst formation. Alternatively, as nutrient stress was already encountered during the acclimation, cyst formation in the remaining cells (which were used for the main study) could have resulted in insufficient reserves for germination and survival of the encysted cell (Anderson and Lindquist 1985), with the costs in energy and nutrient resources needed for encystment outweighing the benefits for cell survival. It is therefore more likely, that the remaining cells used for the main study instead increased storage for metabolite accumulation and were able to continue photosynthesising (Fuentes-Grünewald et al. 2012), resulting in the larger cell volumes (Lei and Lu 2011; Röder et al. 2012; Li et al. 2016) observed under nutrient limited treatments (**table. 3**).

Population growth response

The differences in biovolumes largely correlate to differences in population density (**table 3**), however population biovolume response to pCO_2 differed within nutrient treatments (**fig. 4**). The decreases in biovolume with increasing pCO_2 indicate nutrient limitation to be the limiting factor for population biovolumes under the Limited treatments. Increases in pCO_2 can increase the relative nutrient stress experienced by cells, as an increase in carbon fixation and energy production can increase the nutrient demands of the cell (Graneli and Flynn 2006; Verspagen et al. 2014). Additionally, the Low Limited treatment had relatively lower cell volumes than at higher pCO_2 levels. Smaller cells are limited in their spatial capacity for storing nutrients and have a smaller nutritional requirement than larger cells (Litchman et al. 2007). Therefore, under conditions in which nutrients are of a finite amount, cells of a smaller size (that require less nutrients per cell) could theoretically reach higher population densities than larger cells of the same species under the same conditions.

In comparison, population biovolumes were significantly higher in Replete treatments, except for in the Low treatment where biovolume significantly decreased (**fig. 4**). As nutrients never limiting in Replete treatments, it is likely that C availability became the primary limiting factor for population biomass at the lowest pCO_2 levels. Biovolumes of the Low Replete treatment were also significantly lower than in the Low

Limited treatment, despite population densities being ~45% greater than the Limited treatment. Due to the larger cell volumes seen for the Limited treatments, it is likely that cells put more energy into storage of key metabolites, such as POC quota which was increased under nutrient limitation and would increase cell volumes due to an increased volume of storage vacuoles (Raven 1987; Raven 1997).

Values of μ for *P. reticulatum* from previous studies vary greatly, ranging between 0.14 d^{-1} - 0.29 d^{-1} (Ratti *et al.,* 2007; Montechiaro and Giordano, 2010; Hoins *et al.*, 2015; Hoins *et al.*, 2016; Pierangelini *et al.,* 2017) to 0.32 d^{-1} – 0.52 d^{-1} (Guerrini et al. 2007), the latter being comparable to values obtained in this study (0.36 d^{-1} to 0.45 d^{-1}) (**fig 5**). μ in other phytoplankton groups is indicated to reduce with higher photon intensity. For example, Rost et al. (2002) observed a higher μ for the coccolithophorid, *Emiliania huxyeli*, when exposed to a photon intensity of 80 μmol photons m^{-2} s^{-1} over a photon intensity of 150 μmol photons m^{-2} s^{-1}. Despite being a different phytoplankton group, this could potentially explain the higher μ values indicated in this study (at ~77 μmol photons m^{-2} s^{-1}) as compared to other studies that use photon intensities of ~150 μmol photons m^{-2} s^{-1} (Hoins et al. 2015). Alternatively, differences in μ for the same species may likely stem from slight disparities in experimental set-up that can result in differences of species' metabolic sensitivities to experimental parameters, or intraspecific trait variation. Intraspecific trait variation has been previously exhibited for other dinoflagellate species, such as *A. ostenfeldii* (Brandenburg et al. 2021), and was observed in our pre-experimental trials (**SM1 Pre-experiments**), whereby μ differed between 6 different strains of *P. reticulatum* under the same experimental conditions.

μ remained independent of nutrient treatment (**fig. 5**), forming a strong bell-shaped curve (using all treatments) in response to surface ocean pCO_2 levels of 110 μatm – 698 μatm (R^2 = 0.70; **SM: fig. 15**), with peak growth rates estimated to occur around 420 μatm - 430 μatm comparable to present day conditions. This, along with the highest biovolumes observed in Ambient replete nutrient treatments (**fig. 4**), indicate an optimisation of growth to present day conditions when nutrients are non-limiting. These results for population growth response imply that under projected pCO_2 levels and increases in nutrient limiting situations, such as from enhanced stratification (Gruber 2011; Li et al. 2020), there could be a resulting population biomass loss of some phytoplankton species such as *P. reticulatum,* potentially decreasing the magnitude of fixed and exported carbon to the deep ocean (Falkowski et al. 2000; Sigman and Boyle 2000), therefore negatively impacting on the ocean's buffer capacity to continued increases of pCO_2 levels.

Elemental stoichiometry

Elemental stoichiometry ratios for this study are all within previously recorded ratios for marine phytoplankton (Geider and La Roche 2002; Finkel et al. 2010), and are comparable to ratios obtained from other studies using *P. reticulatum* (Ratti et al. 2007; Montechiaro and Giordano 2010). A slight decrease in POC and PON quota was observed for the Replete Low CO_2 treatment as compared to the two other CO_2 treatments, which become more prevalent when looking at the element-specific growth rate (**fig. 7 D-E**). As well as this, the Low Limited treatment also indicated deviations in POC and PON production, and C:N and

N:P ratios as compared to the higher CO_2 treatments. These decreases of C- and N-related responses for the Low treatments, likely indicate that the lower C availability affected the C assimilation pathway, causing subsequent decreases in PON quota, due to coupling of the C and N assimilation pathway (Flynn 1991; Turpin 1991). As such, the lower C availability likely limits the amount of PGA supply to the TCA cycle, therefore limiting key compounds required for assimilation of N, such as 2-oxoglutarate. These decreases of POC quota and production become more apparent under nutrient limiting conditions as it is likely that cells under this treatment are more severely energy and nutrient limited for sufficient C assimilation.

All nutrient ratios increased under nutrient limitation, indicating changes in accumulation (storage) or depletion of energy (such as carbohydrates and lipids) and nutrient reserves (such as polyphosphate and nitrate), or might indicate changes in functional pools (Geider and La Roche 2002). The overall decreases in PON and POP quota under nutrient limitation likely suggest depletion (or less storage) of N and P reserves due to less environmental nutrient availability (**fig. 3**), whereas increases in POC quota, previously documented for dinoflagellates under nutrient limitation (e.g. Leong and Taguchi 2004; Fuentes-Grünewald et al. 2012; Hoins et al. 2016a), could be the result of increased accumulation of C in storage lipids and carbohydrates (Leong and Taguchi 2004; Fuentes-Grünewald et al. 2012). The higher C:N and C:P ratios under nutrient limiting conditions can indicate the increase in nutrient demands of the cell (due to increased fixation and energy production), suggesting an increase in nutrient limitation stress that the cells experience (Graneli and Flynn 2006; Verspagen et al. 2014). The C:P ratio is commonly used in biogeochemical models to estimate POC production from P concentrations, as drawdown of pCO_2 is driven by a soft tissue pump. A variable C:P ratio is therefore thought to signify a change in strength of the soft tissue pump. Although it could signify that phytoplankton increase C uptake, and insinuate a greater C export, the increased nutrient stress on cells could also result in a lower productivity (due to increases in intracellular C:P and C:N ratios) therefore resulting in future buffering of global carbon export (Matsumoto et al. 2020).

Toxin production

In this study Ambient YTX content did not change with pCO_2 or nutrient treatment, whereas the Low and High treatments documented significant increases and decreases in YTX content, respectively. The YTX contents obtained in the Low Limited treatment is within range with previous studies for *P. reticulatum* under P limiting conditions (~25 pg $cell^{-1}$; (Guerrini et al. 2007)), but this value also incorporates the compounding factor of lower pCO_2 levels, which could explain the relative difference between our much larger increase in YTX relative to the control (~10 pg $cell^{-1}$) than that indicated in Guerrini et al. (2007) of ~2 pg $cell^{-1}$. Additionally, this could also be the result of strain-specific differences in toxin content, indicated to occur for *P. reticulatum* (Paz et al. 2004). To our knowledge, this is the first study of its kind to look either the effect of rising CO_2 levels on toxin content of *P. reticulatum*, or the interactive effects of CO_2 and nutrient limitation on YTX contents of the cell. Despite YTX being a polyether ladder compound (Rein and Borrone 1999; Paz 2008) and in the same category as the more highly known brevetoxin (produced by the Florida 'red tide' dinoflagellate *Gymnodinium breve* (Pierce and Henry 2008)) and ciguatoxin, YTX doesn't appear to

display the same neurotoxic inducing properties, and its mechanism of action is still largely unknown (Paz 2008; Tubaro et al. 2010), proving comparisons with other studies difficult.

This study measured toxin content of the cell and not toxin release, therefore it could also be a possibility that measured cell YTX content did not represent total YTX production if release into the media was significant. In this understanding, it could be that the relatively low [YTX] observed in the High nutrient limited treatment was due to higher release of YTX into the media. Guerrini et al. (2007) found that release of YTX into the media increased under N limitation. Due to the higher CO_2 availability, and resultant greater nutrient requirement, it could be that N limitation is more strongly 'felt' by *P. reticulatum*, therefore increasing the relative N-stress of cells at elevated pCO_2 levels. However, within this understanding, YTX contents of Ambient Limited treatments should also be lower than for Replete treatments due to the relative nutrient limitation, which did not differ in the direct measurements of YTX. Yet, when accounting for cell volume (**SM: fig. 16**) (which was significantly greater at higher pCO_2 levels and under nutrient limitation), values of YTX contents in all Limited treatments decreased relatively, resulting in lower YTX contents in the Limited Ambient treatments relative to the Replete Ambient treatments. This could insinuate that N-stress of cells, resulting in a toxin release, is of greater effect in smaller cells. However, as toxin content in the media was not directly measured, this can only be speculated. Yet an alternative explanation could be that higher CO_2 availability under nutrient limiting conditions, energy is shifted away from toxin production and towards other cellular mechanisms that may promote increased cell survival, such as in maintaining growth rates, for increased nutrient acquisition or C pool leakage reduction

It has additionally been previously suggested that toxin content in *P. reticulatum* increases during the progression from exponential to the stationary phase (Boni et al. 2001; Guerrini et al. 2007; Sala-Pérez et al. 2016), and that maximum YTX toxin release occurs in the stationary phase (Paz et al. 2004; Guerrini et al. 2007; Röder et al. 2012). Some studies even indicate decreases in YTX concentrations over duration of the exponential stage (Röder et al. 2012), which could be an indication of increased energy and nutrient resources allocated to growth. As final measurements for each nutrient treatment were taken during different growth phases (exponential phase for the replete nutrient treatments, and stationary phase for the nutrient limited treatments), this could have an impact on the toxin contents measured. Therefore, we suggest that future studies wishing to investigate climate changes on dinoflagellate such as *P. reticulatum,* should explore further the interactive effects of environmental parameters on toxicity and toxin content, and especially as to how these interactive factors might affect toxin accumulation and/or release during both exponential growth and stationary phase, which could impact the severity of a toxic bloom.

CCMs and carbon isotope fractionation of P. reticulatum

^{13}C fractionation was strongly correlated with increases in pCO_2 for both nutrient treatments over the study, indicating that ^{13}C fractionation is highly CO_2-dependent for *P. reticulatum* under both nutrient limiting and nutrient replete conditions (**fig. 8 C**). ^{13}C fractionation also significantly increased under nutrient limiting

conditions relative to nutrient replete conditions. The preference of ^{12}C by RubisCO is better expressed at higher pCO_2 levels, where CO_2 can be more readily acquired relative to HCO_3^-. This provides implications that *P. reticulatum* increased more CO_2 relative to HCO_3^- under both increases in pCO_2, but also under nutrient limiting conditions. However, as the inorganic C species uptake or CCM activity were not directly measured in *P. reticulatum* in this study, we can only speculate, which we have discussed below.

Other studies have indicated effective CCMs for this species (Hoins et al. 2015), so we therefore cannot rule out this out. The strong negative linear correlations formed for POC production/CO_2 (**fig. 8D**) under both nutrient limiting and nutrient replete conditions could additionally indicate that CCM activity only does not differ significantly between CO_2 treatment, yet the changes in ε_p values would further suggest that modes of CCM differ between nutrient treatments.

A study by Van de Waal et al. (2019) suggested that high CCM activity in earlier evolved phytoplankton groups, such as dinoflagellates, is additionally likely to be accompanied with high CCM plasticity. With increases in environmental inorganic C availability, the energetic costs of carbon acquisition are reduced and down-regulate energy demands of CCMs (Hennon et al. 2015), thereby allowing energy reallocation for nutrient acquisition or growth (Van de Waal et al. 2019). Previous studies have suggested the down-regulation of CCMs in some dinoflagellate species, such as *Alexandrium ostenfeldii* (Van de Waal et al. 2014; Van De Waal et al. 2014; Hoins et al. 2015; Brandenburg et al. 2021), or (Rost et al. 2008; Hoins et al. 2016b), including *P. reticulatum* (Hoins et al. 2016a).

An indication of CCM flexibility to elevated pCO_2 can include higher growth rate and POC production. Additionally, CCM plasticity is thought to only down-regulate CCM activity for higher pCO_2 levels, when CO_2 is in abundance, to perhaps rely primarily on diffusive uptake of CO_2. Yet, under low pCO_2, the correlation between ε_p and carbon demand and supply (POC production and $[CO_{2(aq)}]$) would deviate from being linear, with the possession of CCMs instead supported by a hyperbolic relationship between POC production/$[CO_2]$ and ε_p. At lower pCO_2 levels ^{13}C fractionation decreases due to low carbon supply ($[CO_{2(aq)}]$) and a high carbon demand (POC production), as RubisCO has a lower capacity to discriminate against ^{13}C. A hyperbolic relationship between POC production/$[CO_2]$ and ε_p has previously been described for *P. reticulatum* (Hoins et al. 2015), however Hoins et al. (2015) indicated this hyperbolic relationship using POC quota instead of POC production for the carbon demand, which does not account for growth-related effects.

Contradictory to this, despite *P. reticulatum* within the group considered as earlier evolved phytoplankton, the results from this study are better correlated to a large dominance of diffusive uptake rather than CCM activity. Growth rates in this study did not increase with elevated pCO_2 and remained highest at pCO_2 levels akin to present day (**SM**: **fig. 15**), and POC quota or POC production did not increase with rising pCO_2. Additionally, our study indicates strong linear relationships indicated both between ε_p and $[CO_{2(aq)}]$ (**fig. 8C**), and between ε_p and POC production/$[CO_{2(aq)}]$ (**fig. 8D**). In this case of diffusive uptake, RubisCO ^{13}C fractionation instead changes directly as a function of either carbon supply (growth rate), or carbon demand

(cell size) (Wilkes and Pearson 2019). As growth rates did not increase with pCO_2, and the relationship between POC production to ε_p (**fig. 8B**) decreased in strength relative to the correlation of POC quota to ε_p (**fig. 8A**), increases in ε_p values likely were the result of the function of carbon demand. This is made more plausible due to the large increases in volume indicated for *P. reticulatum,* both at elevated pCO_2, but also under nutrient limiting conditions.

In the purposes of a thorough discussion, to explore all possible scenarios, it is not totally inconceivable that CCMs are significant for inorganic C uptake in this study, which would be possible if data points in this study were constrained by the range of $[CO_{2(aq)}]$ investigated. For example, Hoins et al. (2015) used $[CO_{2(aq)}]$ of ~7 - 45 µmol L^{-1} to result in a curvilinear relationship between carbon supply and demand, whereas the high ^{13}C fractionation of ~27‰ in *A. tamarense* (Wilkes et al. 2017) ~11.5 - 63 µmol L^{-1}. A larger $[CO_{2(aq)}]$ would result in smaller values of POC production/$[CO_{2(aq)}]$, which would perhaps result in values that indicate a 'curve', so it is possible that our results indicated the 'linear' section of the proposed curvilinear relationship. If CCMs are relatively active, as found for *P. reticulatum* previously (Hoins et al. 2015), the differences in ε_p between nutrient treatments could imply changes in the relative uptake of carbon species. Previous studies of *P. reticulatum* report ε_p values of 8‰-10‰ (Hoins et al. 2015), comparable to those seen in replete nutrient treatments of this study which range from 7.65‰ to 10.42‰. Hoins et al. (2016b) indicated use of CO_2 and HCO_3^- in equal proportions under nutrient replete conditions, therefore it could be that under nutrient limited conditions, there is either reduced production and/or functioning of CCMs. Decreased functioning and production of CCMs could be the result of severe nutrient limitation through decreases/cease of energy allocation, synthesis of proteins, nucleic acid and DNA/RNA.

Tthe greater ε_p values in nutrient limited treatments might not only be due to an increased CO_2 contribution, but could also be intensified to an increase in leakage. Leakage can result in increases of ε_p values, as higher leakage replenishes the intracellular inorganic C pool. This can therefore decrease accumulation of ^{13}C in the locality of RubisCO (Sharkey and Berry 1985; Rost et al. 2006a). therefore increasing the fractionation, and is associated with greater CO_2 contributions to ^{13}C fractionation. Although *P. reticulatum* has been previously shown to have low leakage values that remain independent of pCO_2 (Hoins et al. 2016b), this was under nutrient replete conditions. It remains a possibility that nutrient limitation could increase the relative cost of maintaining the internal C pool, resultantly increasing leakage.

As well as higher ε_p values, the slope of ε_p relative to pCO_2 under nutrient limited treatments (0.38‰ (µmol L) $^{-1}$) is also greater than in replete nutrient treatments (0.11‰ (µmol L) $^{-1}$). This shows that sensitivity of ε_p to $[CO_{2(aq)}]$ increases with an increase in CO_2 availability under nutrient limiting conditions. Other dinoflagellate studies have indicated a comparable slope, such as for *Alexandrium tamarense* (0.11‰ (µmol L) $^{-1}$), *Gonyaulax spinifera* (0.17‰ (µmol L) $^{-1}$) and *S trochoidea* (0.16‰ (µmol L) $^{-1}$) (Hoins et al. 2015), and the coccolithophorid, *E. huxleyi*, (~0.13‰ (µmol L) $^{-1}$; (Rost et al. 2002)). However, studies with *P. reticulatum* have observed slopes of ε_p to $[CO_{2(aq)}]$ at around 0.05‰ (µmol L) $^{-1}$ under nutrient replete conditions (Hoins

et al. 2015)), a value much lower than what this study obtained (0.11 ‰ (µmol L) $^{-1}$). There could been strain-specific differences to uptake of carbon species (Brandenburg et al. 2021), resulting in a lower sensitivity of ^{13}C fractionation by RubisCO to changes in pCO_2 in the strain of *P. reticulatum* used by Hoins et al. (2015). Additionally, Hoins et al. (2015) looked over a larger CO_2 range, closer to 50 µmol L^{-1}, whereas this study observed $[CO_{2(aq)}]$ of <25µmol L^{-1}. It has been shown that at higher concentrations ε_p values can start to plateau or be lower after CO_2 concentrations greater than 30-40 µmol L^{-1} (Hinga et al. 1994; Hoins et al. 2015), which can alter a linear gradient. This is also indicated for *A. tamarense,* which increased ε_p values by ~5‰ over ~12 µmol L^{-1} (from ~11.5 – 23.7 µmol L^{-1}), but then increased relatively less by ~6‰ over ~39 µmol L^{-1} at higher $[CO_{2(aq)}]$ (~23.7 – 63 µmol L^{-1}) (Wilkes et al. 2017). Therefore, it is conceivable that the larger range of $[CO_{2(aq)}]$ investigated in the study by Hoins et al. (2015) altered the slope of the linear gradient relative to our own.

The results of this research contradict previous studies that use *P. reticulatum,* in that the significant functioning of a CCM to C uptake is not witnessed, even at low $[CO_{2(aq)}]$, along with an apparent lack of down-regulation of CCMs at elevated pCO_2. This study additionally points towards diffusive uptake as the dominant pathway for inorganic C uptake, which due to the high sensitivity of ε_p changes in pCO_2, likely independent of growth rates, is advantageous in the investigation toward $\delta^{13}C$ dinocyst as a proxy for CO_2.

The dinocyst $\delta^{13}C$ palaeo-CO_2 proxy

Recent works have proposed the use of fossilised species-specific dinocyst $\delta^{13}C$ as a novel proxy for palaeo-CO_2 (Hoins et al. 2015).The general results of a strong CO_2-dependency of ^{13}C fractionation and potential dominance of diffusive uptake for carbon uptake, under both nutrient replete and nutrient limiting conditions by *P. reticulatum,* implies that ^{13}C signatures of this species' dinocysts have great potential for the reconstruction of past CO_2 concentrations. However, it remains that potential external and/or internal factors can influence the ε_p signal. We will subsequently discuss these alongside the implications of this research to a dinocyst $\delta^{13}C$ CO_2 proxy whilst highlighting potential constraints of this research, before making concluding remarks.

As nutrient limitation is a trigger for cyst formation by *P. reticulatum* (**SM1 Preliminary experiments**), and our results indicate that ε_p signals both increase in value and sensitivity under nutrient limiting conditions, it highlights interesting insights into the role of nutrient availability on the dinocyst $\delta^{13}C$ sedimentary signal. The increased sensitivity of ε_p to $[CO_{2(aq)}]$ under nutrient limiting conditions could indicate that *O. centrocarpum* (*P. reticulatum* dinocysts) have large sensitivity of ε_p to $[CO_{2(aq)}]$, as formation would occur at point of nutrient limitation. This could be beneficial as its use as a CO_2 proxy as changes in pCO_2 would be recorded in the $\delta^{13}C$ signatures, but to a greater extent than cells under nutrient replete conditions. However, this must be considered when attempting to reconstruct past pCO_2 levels, as if cyst formation is not triggered by nutrient limitation, it could lead to an overestimation of pCO_2 levels. However, our results additionally indicate that if ε_p signals are found to be above ~11‰, they are likely the result of nutrient-

limiting conditions as trigger of cyst formation, as ε_p values did not increase to above this level for cells under nutrient replete conditions.

This study used a [$CO_{2(aq)}$] range of 3.58 ± 0.40 µmol kL^1 to 22.83 ± 1.24 µmol L^{-1}, and it is unknown if ε_p signals for this strain of *P. reticulatum* would increase further under higher [$CO_{2(aq)}$] under nutrient replete conditions. Yet ε_p signals are estimated to only reduce in sensitivity between 30-40 µmol L^{-1}, which could allow reconstructions covering the Cenozoic era, which encompasses large climate variations and is thought essential increase our understanding of carbon cycling to our climate system using palaeo-environmental studies. In addition, this proxy could either help reinforce previous proxies, or cover eras with which current proxies have relatively largely ambiguous, such as the period between 40-50 Mya (Mid Eocene) where proxies such as liverworts, stomata and nahcolite-trona are contradictory and have large uncertainties. The maximum reach of *O. centrocarpum* in the sediment record is ~65 Mya (REF), so this could potentially cover many events of palaeo-significance, such as Palaeocene-Eocene Thermal Maximum (PETM; ~56 Mya), where the global temperatures increased by more than 5˚C in over less than 10,000 years (Dunkley Jones et al. 2013; Frieling et al. 2017). Additionally, where other dinoflagellate species limit in CO_2 sensitivities at low pCO_2 concentrations due to influence of CCMs on ^{13}C fractionation, *P. reticulatum* likely is advantageous as the influence of CCMs to the CO_2-dependent ε_p signals are either negligible or lacking, such as seen during the Middle Miocene (~15 Mya),

Due to the common-place use of this species in biostratigraphy (e.g. , use of this species for a proxy would be beneficial as not only could the dinocysts be used for CO_2 predictions, but the same fossils could be directly linked for biostratigraphic studies (Santos et al. 2017) as this species undergoes distinct morphological changes in response to environmental conditions, such as different salinities and temperatures (Mertens et al. 2011; Verleye et al. 2012; Jansson et al. 2014). It is indicated that below the Pliocene the morphotypes start to widen in variation into the lower Neogene and Palaeogene (Verhoeven and Louwye 2012; De Schepper et al. 2017) Therefore, it could provide constraints if these strain-specific differences do not occur just morphologically but also physiologically. For example, if methods of inorganic C uptake is shown to be significantly different for strains of *P. reticulatum,* this can therefore impact of the relative contribution of CO_2 or HCO_3^- to the ε_p signal. This could then result in overestimation or underestimation of dinocyst $\delta^{13}C$, subsequently increasing uncertainty to calculated pCO_2 reconstructions.

Growth rates are difficult to constrain from palaeo-reconstructions (Popp et al. 1997), yet this study indicates ^{13}C fractionation to be directly related to cell size and not influenced by growth rate. This could provide advantageous over other species, where growth rates are indicated to influence ^{13}C fractionation (Laws et al. 1995; Laws et al. 1997; Laws et al. 2002).

We cannot overlook the fact that cyst formation in this study was negligible, proving them statistically unviable for measurements of ε_p. However, a brief investigation into the difference between ε_p signals of the nutrient limited and nutrient replete treatments at a specific pCO_2, indicated a likely quantifiable

relationship with pCO_2 (**SM: fig. 17**). The difference in mean ε_p between the nutrient limited and nutrient replete treamtents at a given pCO_2 level increased by 14% with a ~2-fold increase in pCO_2 levels (14.2% for a 1.95-fold increase between Low and Ambient treatments; 14.4% for a 2.2-fold increase between Ambient and High treatments). However, it must be taken into consideration that: 1. we are using cells for this quantification; 2. there are not enough data points to be statistically viable and 3. pCO_2 measurements were indicated to significantly differ between nutrient treatments of the Ambient CO_2 treatment. However, although this correlation cannot be used in practice, it indicates a possible relationship for ε_p signals under nutrient limiting conditions and ε_p signals under nutrient replete conditions. However, it remains that direct cyst-cell comparisons are essential to investigate the potential isotopic offset (if any) at varying pCO_2 levels.

Concluding remarks

We have used semi-closed experiments to indicate the strong correlations of ^{13}C fractionation to pCO_2, and increased ε_p-sensitivity to pCO_2, under nutrient limiting conditions for *Protoceratium reticulatum,* likely due to predominance of diffusive uptake for inorganic C uptake over inorganic carbon acquisition by CCMs. We additionally observe that POC quota and cell size likely relate to ^{13}C fractionation, more so than growth rate of which the affects were unapparent. These results also give insight that *Protoceratium reticulatum* provides many reasons as to why further studies should use it as a model species with which to further investigations towards fossil dinocyst $\delta^{13}C$ as a novel palaeo-CO_2 proxy. Few of these include its prevalence in the sediment record, the apparent non-influence of growth on inorganic C uptake, sensitivity of ^{13}C to CO_2 availability at low pCO_2 and obvious morphology. If successful could provide valuable resolution to contradictions in the pCO_2 record up to the Cenozoic. Additionally, due to the cosmopolitan nature of this species, it is highly likely that strain specific differences could affect ^{13}C fractionation, providing a diverse model with which to indicate any relationships that may occur between distinct strains.

Acknowledgements

I would like to thank Dr. Karen Brandenburg for her awesome guidance and introducing me to this subject, of which I had very little knowledge before. I would like to also thank her for the excellent supervision she provided throughout my Master thesis, but especially for her answers to my many questions.

Of course, special thanks must go to the team at NIOO-KNAW, who allowed me to undertake in this study, both during and after the COVID-19 restrictions. More specifically, I would like to thank Nico Helmsing who gave consistent guidance to experimental technicalities and for the sample analyses.

Additional thanks must go to Dr. Thijs Frenken and Dr. Dedmer van de Waal for their guidance at NIOO-KNAW.

A special thanks also goes to Dr. Appy Sluijs, for his guidance as my supervisor at the University of Utrecht and for introducing me to Karen.

I would like to also give a huge thanks to the students at Wageningen University and to everyone at Ecodorp Ppauw, who welcomed my van and me in to stay with them.

Lastly, I thank Chella and Dennis for their support within the Netherlands, and my friends and family back in the UK for their continual support and flapjack throughout this thesis

Supplementary material (SM)

Contents

SM1: Pre-experiments

Working hypothesis

The initial aim of this thesis was to investigate the relationship of carbon isotope fractionation between the cell and cyst of a dinoflagellate. For now, there is no standard framework enabling dinoflagellate cyst formation under experimentally controlled conditions. Therefore, trials prior to the main experiment explored species cyst formation under varying nutrient limiting condition and experimental set-ups that focused on highest possible cellular (and cyst) biomass alongside minimal fluctuations of carbonate chemistry. The species used were single strains of *Lingulodinium polyedrum* and *Pyrodinium bahamense,* and 6 strains of *Protoceratium reticulatum.* Trials took place over the course of 4 months (Oct 2020 – Feb 2021) prior to the main experiment.

Sample and observation days were limited due to laboratory restrictions involving COVID-19.

Materials and method

For greater detail surrounding methods of cell counts, growth rate calculations or materials in these pre-experiments, refer to the Materials and Methods of the main study, which should provide sufficient detail.

Species and culture media

Stock cultures of *L. polyedrum, P. reticulatum* and *P. bahamense* were maintained in the indicated culture media, temperatures, and salinities (**table. 1**).

SM: Table 4: Stock culture conditions, including details of media, growth temperature and salinities used. For ingredients of culture media, **see SM: table 2**

Species	Strain	Location of origin	Temperature (˚C)	Salinity (psu)	Culture media
P. reticulatum	VD5.2	Concarneau, France	16	36	f/2 replete
	VD2	Concarneau, France	16	36	f/2 replete
	CCCAE	Concarneau, France	16	36	f/2 replete
	4BF	Concarneau, France	16	36	f/2 replete
	F6	Concarneau, France	16	36	f/2 replete
	ONO3	Concarneau, France	16	36	f/2 replete
L. polyedrum		Concarneau, France	16	36	f/2 replete
P. bahamense			24	25	Ge/s replete

Volumes of stock cultures and media were dependent on the culture density and initial cell density of the experiment.

$$V_{culture} = \frac{N_0 + V_{total}}{N_{culture}} \quad (1)$$

$$V_{media} = V_{total} + V_{culture} \quad (2)$$

Where N_0 is initial experimental cell density and $N_{culture}$ is cell density of the stock culture. V_{total} is the experimental volume (e.g. 50mL in inoculations), and $V_{culture}$ and V_{media} are the volumes of the stock culture and additional media respectively.

For ease of reading, the individual reasoning and methods for each trial are given in order of execution. Results and brief analysis are given simultaneously, subsequent to the methods.

SM: Table 5: Details and ingredients of experimental media used in the pre-experiments.

Medium name	Salinity	Base media ingredients	Limited nutrients *
f/2 replete	36	North Sea water; Trace metals and vitamins[a]; H_2SeO_3[b]	-
f/2 P lim	36	North Sea water; Trace metals and vitamins[a]; H_2SeO_3[b]	P
f/2 N lim	36	North Sea water; Trace metals and vitamins[a]; H_2SeO_3[b]	N
f/2 NP lim	36	North Sea water; Trace metals and vitamins[a]; H_2SeO_3[b]	N, P
Dilute f/2 replete	25	North Sea water; Trace metals and vitamins[a]; H_2SeO_3[b]; Milli-Q[c]	-
Dilute f/2 P lim	25	North Sea water; Trace metals and vitamins[a]; H_2SeO_3[b]; Milli-Q[c]	P
Dilute f/2 N lim	25	North Sea water; Trace metals and vitamins[a]; H_2SeO_3[b]; Milli-Q[c]	N
Gse/4 replete	25	North Sea water; Trace metals and vitamins[d]; H_2SeO_3[b]; Milli-Q[c]	-
Gse/4 P lim	25	North Sea water; Trace metals and vitamins[d]; H_2SeO_3[b]; Milli-Q[c]	P
Gse/4 N lim	25	North Sea water; Trace metals and vitamins[d]; H_2SeO_3[b]; Milli-Q[c]	N
Gse/4 NP lim	25	North Sea water; Trace metals and vitamins[d]; H_2SeO_3[b]; Milli-Q[c]	N, P

[a] added according to f/2 media (Guillard and Ryther 1962)
[b] added according to K medium (Keller et al. 1987)
[c] diluted with Milli-Q to reach salinity of 25 psu
[d] added according to Gse/4 media from (Blackburn et al. 2001)
* Nutrients excluded relative to f/2 medium, where N is limited within $NaNO_3$; P is limited within $NaH_2PO_4 \bullet 2H_2O$

Inoculations

All inoculations were performed in 50mL/25cm^2 sterile cell culture flasks, which were kept in incubators at constant temperatures (16˚C for of *L. polydrum* and *P. reticulatum;* 24˚C for *P. bahamense*) with light:dark cycle of 16:8 h. Initial cell densities vary for inoculations, and a summary of trial conditions can be found in SM: Table. 3.

INO1: Species cyst-formation of 3 different species

Initial inoculations explored the cyst-forming abilities of *L. polydrum, P. reticulatum* strain VD5.2 and *P. bahamense.* Species were inoculated for a duration of 59 days in dual nutrient limited media (f/2 NP lim for *L. polydrum* and *P. reticulatum* strain VD5.2; Gse/4 NP lim for *P. bahamense*) at initial cell densities of 40 cells mL^{-1}.

INO2.1: Nutrient limitation and cyst formation

The effect of nutrient limitation of a single nutrient on cyst formation on *P. bahamense, L. polyedrum* and *P. reticulatum* strain VD5.2 was explored. *L. polyedrum* and *P. reticulatum* strain VD5.2 were each inoculated in f/2 P lim, f/2 N lim and compared with f/2 replete. Initial cell densities were 40 cells mL^{-1}. Inoculations under f/2 N lim ran for 48 days, whereas inoculations under f/2 P lim ran for a total of 51 days.

INO2.2: P. bahamense growth in f/2 medium.

To maintain consistency of media and for the purposes of experimental controls, the growth of *P. bahamense* was also explored in a f/2-based media (dilute f/2 replete) diluted with Milli-Q, with a salinity of 25. Simultaneously, *P. bahamense* was inoculated in dilute f/2 P lim and dilute f/2 N lim and compared with growth in dilute f/2 replete. All these inoculations ran for a duration of 13 days.

INO3: Cyst formation of additional P. reticulatum strains.

Due to the success of *P. reticulatum* strain VD5.2 cyst formation in pre-experiments INO1 and INO2, the cyst-forming abilities of additional *P. reticulatum* strains (F6, ONO3 and VD2) were explored. The three *P. reticulatum* strains were inoculated in f/2 NP lim at an initial cell density of 40 cells mL^{-1} for a duration of 21 days (*P. reticulatum* strains ONO3 and VD2) or 28 days (for *P. reticulatum* F6).

INO4: Investigating a larger N_0

The impact of a larger initial cell density on rate of cyst formation and cell growth was explored for all species and strains used in previous inoculations, with the additional two more strains of *P. reticulatum* (CCCAE and 4B7) under the same conditions. Initial cell density of all species and strains was 100 cells mL^{-1}, and the trial ran for a duration of 28 days for all strains, except *P. reticulatum* strain 4B7, which ran for 31 days, and *P. bahamense,* which ran for 13 days. All species and strains were grown in f/2 NP lim, except *P. bahamense,* which was grown in Gse/4 NP lim.

INO5 – Very high initial cell densities.

A very high initial cell density was explored (t = 26 days) with *L. polyedrum* and *P. reticulatum* strain F6, where N_0 = 459 cells mL^{-1} and N_0 = 682 cells mL^{-1} respectively.

Aeration trials

As referred to in the thesis introduction, previous studies with dinoflagellate growth are commonly limited in maximum cell densities due to changes in carbonate chemistry from inorganic C consumption during photosynthesis. Dinoflagellates are known for their sensitivity to turbulence (Thomas and Gibson 1990), therefore aeration trials were to investigate species tolerance to low continuous gas flow into the media (and therefore bubbling). This direct input of pCO_2 into the media is to enable quicker diffusion of carbonate species, which could aid towards minimising fluctuations in the carbonate chemistry at high cell biomass (>400 cells mL^{-1}).

Cultures were grown in airtight 1L borosilicate bottles with gas flow enabling sealed tops, whereby a continuous gas flow of the pre-mixed pCO_2 was input through a low flow rate of <0.1L/h (for experimental set up of bottles, refer to the main thesis text **fig. 2**).

Counts were done for estimates of growth rate and population growth responses to aeration. Live samples were occasionally taken for visual analysis of motility and morphologies for any indication of stress. Each subheading summarises the specific reasoning and method for additional understanding of each aeration trial beyond this description.

AIR1- Species growth and tolerance

Cultures of were grown under nutrient replete conditions to assess species-specific tolerances to turbulence and bubbling, with a low flow rate of continual gaseous input at ambient pCO_2 levels. Due to spatial limitations at the time of experimentation, this trial was split into 3 groups which were run in succession of each-other. All initial cell densities were 100 cells mL^{-1}, but trials differ between the time at which they ran for, indicated below:

AIR1.1: *P. reticulatum* strain VD5.2, *L. polyedrum,* and *P. bahamense;* trial ran for 11 days,

AIR1.2: P. reticulatum strains VD2 and ONO3; trial ran for 34 days,

P. reticulatum strain F6, and *L. polyedrum*; trial ran for 26 days,

AIR1.3: P .reticulatum strains 4B7 and CCCAE; trial ran for 25 days .

AIR2- Species growth and cyst formation

Cultures were grown under nutrient limited conditions to observe the cyst-forming abilities of strains and species under nutrient stress and a continual low flow rate of gaseous input at ambient pCO_2 level. A low (70 cells mL^{-1}) and high (300 cells mL^{-1}) initial cell densities were also used for each strain, as we were looking to cause mass cyst formation which might be encouraged under population densities relative to peak bloom densities in nature.

The trial including *P. reticulatum* strain F6 and VD5.2 ran for a duration of 17 days, whereas the trial investigating cyst formation for *L. polyedrum* and *P. reticulatum* strain 4B7 ran for 11 days.

SM: Table 6 | Summary of trials and observations. Where P. ret = P. reticulatum, L.poly. = L. polyedrum, and P. bah. = P. bahamense; t = time in days; N_0 = initial cell density; Obs = observations only, with no cell or cyst counts. For details of media, refer to **Table. 2**

Trial Code	Species [strain]	Media	N_0	t	Final cell density (cell mL^{-1})	Final cyst density (cyst mL^{-1})	Observations
Inoculations							
INO1	*P. ret.* [VD5.2] *	f/2 NP lim	40	59	157	407	Plenty of cyst formation under nutrient limitation; Mobile cells look healthy; clear cysts, appear to clump/stick together
	L. poly.	f/2 NP lim	40	59	980	<1	17 cysts $50mL^{-1}$.; cysts look healthy; many cells still active; much DOM
	P. bah.	Gse/4 NP lim	40	22	380	0	Many stress bubbles on cells; disfigured cells; looks unhealthy; much DOM
INO2.1	*P. ret.* [VD5.2] *	f/2 N lim	40	48	Obs.	Obs.	Many cells motile; some cells clumped and immotile but still alive; many cysts; all cysts look abnormal/non-uniform (not spherical) – strange shapes as if no structure to cell wall; cyst walls look thinner than for P lim; smaller cysts as compared to those formed under f/2 P lim or f/2 NP lim
	P. ret. [VD5.2] *	f/2 P lim	40	51	376	500	Many cysts; cyst clumping; profiles disfigured on many; Appearance similar to cysts formed under f/2 NP lim media.
	L. poly.	f/2 N lim	40	48	Obs.	Obs.	Observation only, no formal cell count. Lots of dead cells / OM.
	L. poly.	f/2 P lim	40	51	1080	0	Many disfigured; much DOM; some swimming
INO2.2	*P. bah.*	Dil. f/2 replete	40	13	538	0	Much OM; swimming cells attached in pairs or 4s; many disfigured/swelled cells
	P. bah.	Dil. f/2 N lim	40	13	754	0	Many cells alive but immotile; chains of 2s or 4s
	P. bah.	Dil. f/2 P lim	40	13	566	0	Some stress response bubbles; cells in chains of 2s or 4s; many disfigured cells
INO3	*P. ret.* [F6] *	f/2 NP lim	40	28	1056	35	Cysts not much bigger than cells, many cysts
	P. ret. [ONO3]	f/2 NP lim	40	21	1188	0	Lots of activity; not much indication of encystment
	P. ret. [VD2]	f/2 NP lim	40	21	1350	0	Not much indication of encystment, few larger and rounded/swelled cells, some immotile cells that are still alive. Many 'burst' cells and dead cells.
INO4	*P. ret.* [VD5.2] *	f/2 NP lim	100	28	608	60	Some cysts formed; some swimming
	P. ret. [F6] *	f/2 NP lim	100	28	1120	120	Many cysts; cyst profiles longer than those seen in *L. poly* and *P. ret* VD5.2; many immotile cells still alive
	P. ret. [ONO3]	f/2 NP lim	100	28	Obs.	Obs.	Many cells dead; live ones slow moving; much deformity
	P. ret. [VD2]	f/2 NP lim	100	28	Obs.	Obs.	Many dead/burst cells; live ones slow moving; lots of debris/OM; some stress bubbles and deformation
	P. ret. [4B7]	f/2 NP lim	100	31	1460	<1	20 cysts 50 mL^{-1}

	P. ret. [CCCAE]	f/2 NP lim	100	19	1232	0	Most cells alive on the base appear unable to swim; cells have swelled in size and disfigured.
	L. poly.	f/2 NP lim	100	28	1082	<1	3 cysts 50 mL^{-1}; cells very active
	P. bah.	Gse/4 NP lim	100	13	Obs.	Obs.	Many deformed cells, don't look healthy; no cysts.
INO5	*P. ret.* [F6] *	f/2 NP lim	459	13	1668	Many*	Too many cysts observed to count; many motile cells
	L. poly.	f/2 NP lim	682	26	850	<1	16 cysts in 50 mL; cysts have strange profiles; many immotile cells; cells appear larger/swelled as compared to replete
Aeration trials							
AIR1.1	*P. ret.* [VD5.2]	f/2 replete	100	11	2648	0	Culture and cells look healthy
	L. poly.	f/2 replete	100	11	283	2	A couple of cysts; cells look healthy
	P. bah.	Gse/4 replete	100	11	18	0	Most disfigured; no cysts
AIR1.2	*P. ret.* [F6]	f/2 replete	100	26	28200	0	Healthy cells; lots of growth; very dense
	P. ret. [ONO3]	f/2 replete	100	26	16800	0	Healthy cells; dense growth under aeration
	P. ret. [VD2]	f/2 replete	100	26	16040	0	Healthy cells; dense growth under aeration
	L. poly.	f/2 replete	100	26	10280	0	Base of bottle covered in cells before disturbing – maybe many immotile?
AIR1.3	*P. ret.* [4B7]	f/2 replete	100	25	8960	0	Dense growth under aeration
	P. ret. [CCCAE]	f/2 replete	100	25	15400	0	Dense growth under aeration
AIR2	*P. ret.* [VD5.2] *	f/2 NP lim	70	17	88	4	Good cyst growth under nutrient limitation and aeration
	P. ret. [VD5.2] *	f/2 NP lim	300	17	324	42	Sufficient cyst growth under nutrient limitation and aeration; sufficient cell density for potential further analysis
	P. ret. [F6]	f/2 NP lim	70	17	113	0	No cysts seen in the count chamber
	P. ret. [F6] *	f/2 NP lim	300	17	520	16	Sufficient cyst growth under nutrient limitation and aeration; good cell density for potential further analysis
	L. poly.	f/2 NP lim	70	11	126	0	No cysts in the counting chamber
	L. poly.	f/2 NP lim	300	11	636	0	No cysts in the counting chamber
	P. ret. [4B7]	f/2 NP lim	70	11	50	0	No cysts in the counting chamber
	P. ret. [4B7]	f/2 NP lim	300	11	213	0	No cysts in the counting chamber

* Trials that resulted in a good cyst formation density

Results

A full summary of cell and cyst counts, along with noted observations, can be found above in (**table. 3**).

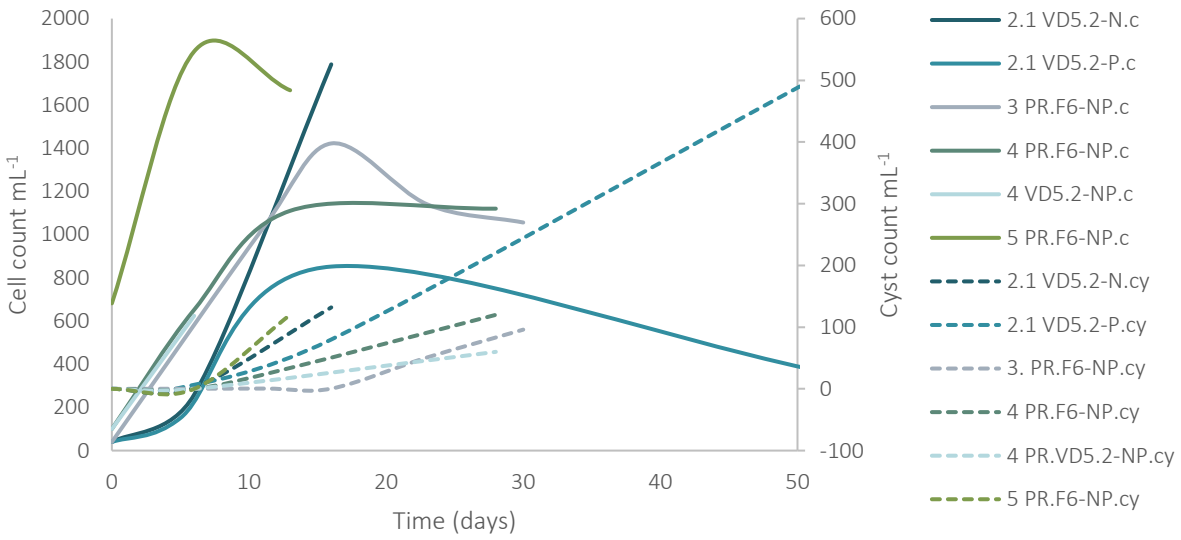

SM: Figure 10 | Cell and cyst counts for P. reticulatum strains that indicated significant cyst formation during inoculations. Cell counts are on the primary y axis, and indicated with solid lines, cyst counts are indicated with dashed lines. Legend labels indicate inoculation number (e.g. 3 = INO3), species (PR = P. reticulatum; F6 or VD5.2 indicate strain identification), nutrient conditions (-N = N limitation, -P = P limitation, -NP = N and P limitation) and if cell (c) or cyst (cy) counts.

All strains and species grew sufficiently under both nutrient limiting and nutrient replete conditions, except *P. bahamense,* which did not grow well in either dilute f/2 replete or Gse/4 replete treatments. Significant cyst formation did not occur for *L. polyedrum, P. bahamense, P. reticulatum* strains CCCAE, VD2, 4B7 and ONO3 therefore we did not proceed with this species for the results analysis. These results indicate not only species-specific responses to growth, but also strain-specific responses to growth and cyst formation.

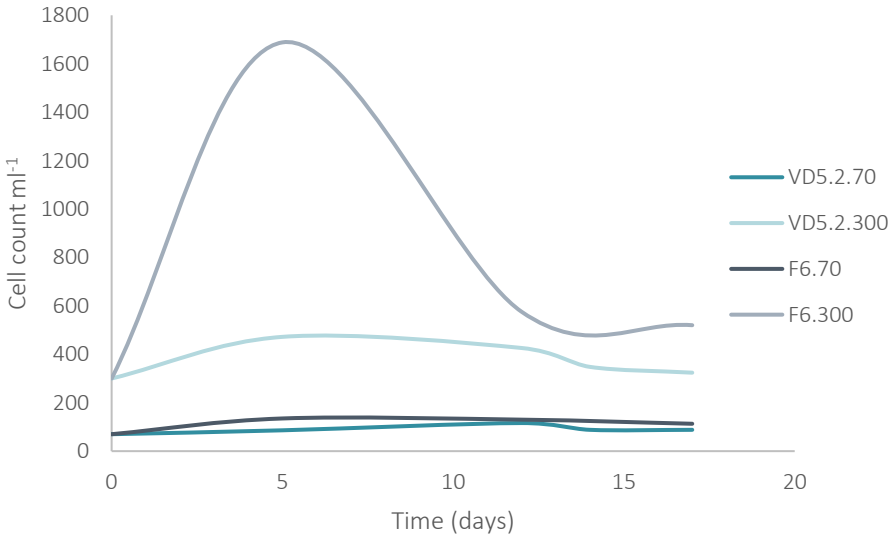

SM: Figure 11 | Cell counts under aeration treatment. Legend indicated the *P. reticulatum* strain, with the corresponding initial cell density (70 cells mL^{-1} or 300 cells mL^{-1})

For the purposes of readability, *P reticulatum* strain F6 and *P. reticulatum* strain VD5.2 will be abbreviated to F6 and VD5.2, respectively, for the remainder of the pre-experiments.

Cyst formation for both VD5.2 and F6 were significant (**SM: fig 10**) and were therefore used for aeration trials. Cell densities reached a peak and declined during which cyst formation increased. Cell densities under P limiting conditions were shown to continually decline for VD5.2, whereas dual N and P limitation resulted in cell densities declining before reaching a plateau.

Population growth under aeration was greatest for F6 with initial start densities of 300 cells mL^{-1} (**SM: fig 11**), but a large decline in density is observed before levelling out. As similar amounts of cyst formation were seen for both VD5.2 and F6 (**SM: table 6**), it is potential that the large peak and decline in population of F6 indicate cell mortality, rather than cyst formation. Therefore, we will proceed with VD5.2 for the main study.

SM2: Supplementary Material – Main Experiment

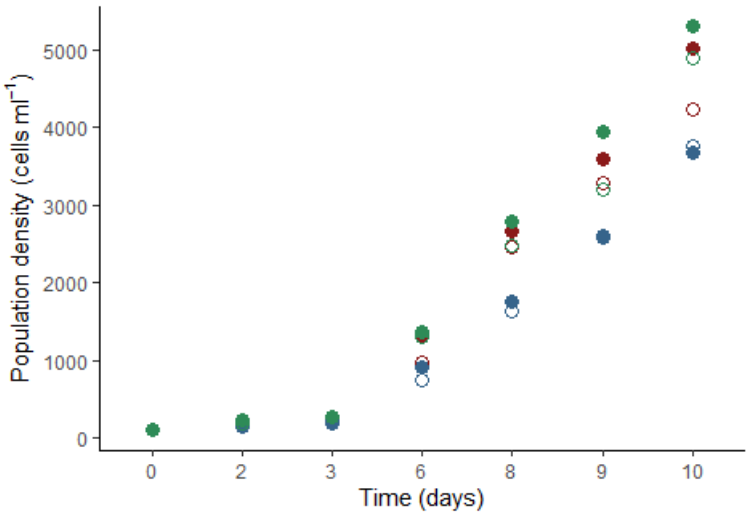

SM: Figure 12 | Population densities during study acclimation. Cultures were acclimated to low (green), ambient (blue) and high (red) CO_2 treatments under nutrient replete (solid) or nutrient limited (hollow) media.

SM: Table 7 | pH and temperature sampling days

Nutrient replete	Nutrient limited
0, 2, 4, 6, 7, 8, 9, 10, 11	0, 2, 4, 6, 8, 10, 12, 15, 18, 20, 22, 26, 29, 32, 36, 40, 42

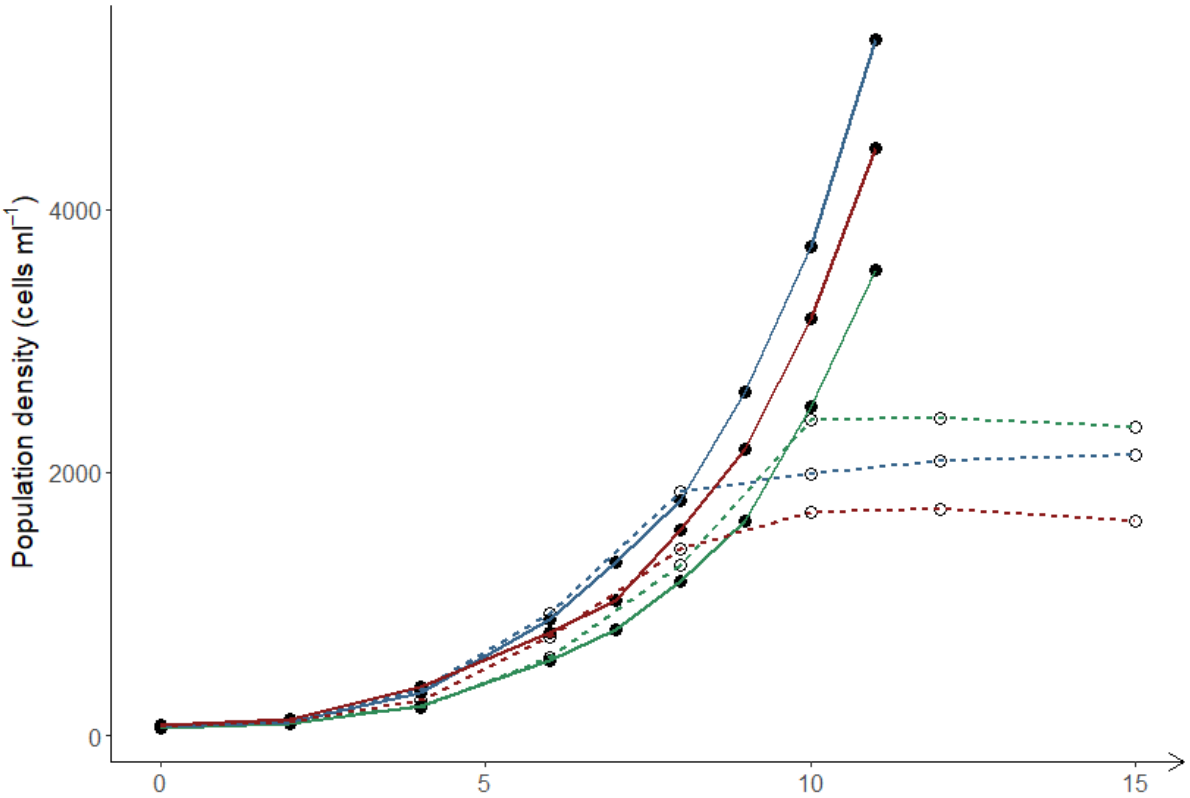

SM: Figure 13 | Measured population densities over time. Different colours represent the respective pCO_2 treatments, where red, blue and green circles represent the triplicate means of High, Ambient and Low treatments, respectively. Solid lines and filled circles represent the nutrient replete treatments, dashed lines with hollow circles represent the nutrient limited treatments. The arrow on the x axis indicates continuation of the limited treatment to day 42, but values are not shown for ease of visualisation.

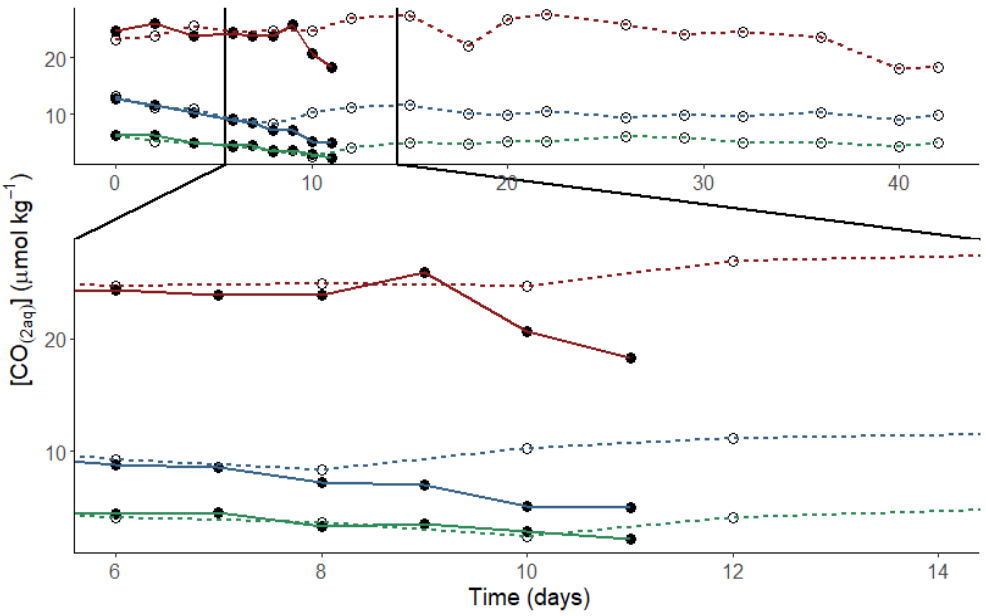

SM: Figure 14 | $CO_{2(aq)}$] for experiment duration. Different colours represent the respective pCO_2 treatments, where red, blue and green circles represent the triplicate means of High, Ambient and Low treatments, respectively. Solid lines and filled circles represent the nutrient replete treatments, dashed lines with hollow circles represent the nutrient limited treatments. The section-zoom shows the area from day 8-10 where [$CO_{2(aq)}$] of treatments starts to deviate.

SM: Table 8: Cell size measurements

Nutrient regime	CO_2 treatment	Width (µm)			Length (µm)			Volume (µm³)		
		Min	Max	Mean	Min	Max	Mean	Min	Max	Mean
Replete	Low	17.3	30.71	**25.11**	24.1	41.41	**33.16**	3788	19959	**11222**
	Ambient	19.05	34.67	**26.73**	24.98	46.19	**35.47**	4752	27052	**13558**
	High	19.3	35.01	**27.81**	27.11	45.58	**37.03**	5463	27546	**15238**
Limited	Low	20.25	39.88	**30.19**	25.24	50.87	**37.89**	5419	40027	**18715**
	Ambient	21.59	37.73	**30.53**	27.21	48.66	**38.92**	7022	39912	**19756**
	High	24.23	40.08	**33.16**	30.37	52.47	**41.67**	9437	42098	**24702**

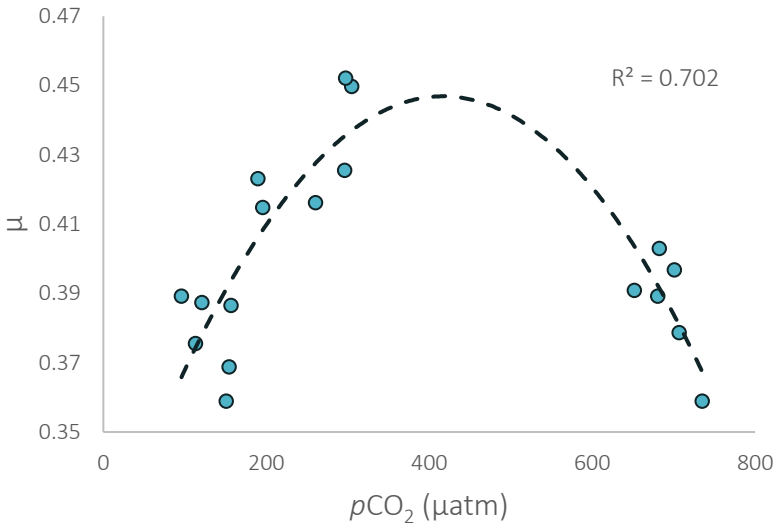

SM: Figure 15 | Specific growth rate of *P. reticulatum* as a function of pCO_2

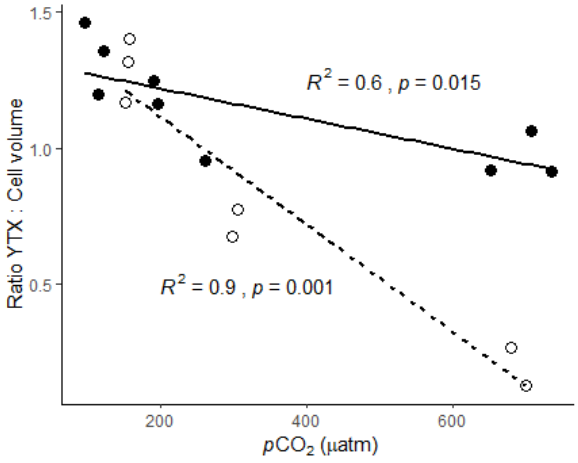

SM: Figure 16 | Ratio between YTX concentration (fg cell^{-1}) and cell volume (µm^3) as a function of pCO_2. Replete nutrient treatments are indicated by hollow circles with solid lines of best fit, and limited nutrient treatments are indicated with filled circles and dashed best fit lines.

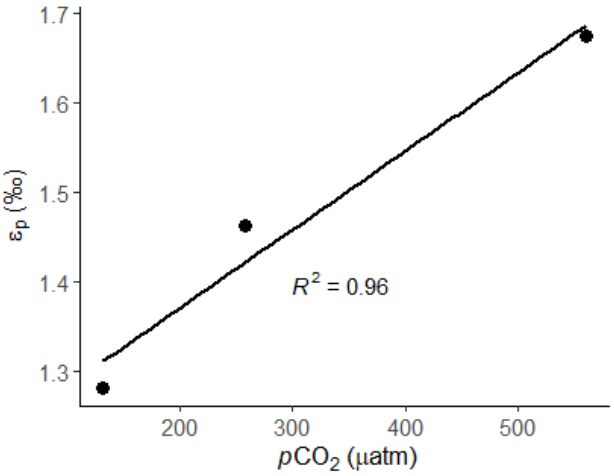

SM: Figure 17 | The calculated difference of triplicate mean ε_p between nutrient replete and nutrient limited cells of *P. reticulatum* in each CO_2 treatment

Appendix I

Dinoflagellate life cycles

Most dinoflagellate species exhibit a haplontic life cycle, where mitotic division occurs in the haploid stage and a zygote is the diploid stage (Pfiester and Anderson 1987), few exceptions such as *Notiluca* (Fukuda and Endoh 2006), and potentially *Polykrikos kofoidii*, (Tillmann and Hoppenrath 2013). The most common sexual cycle includes haploid vegetative cells that differentiate to gametes, which in turn fuse into a diploid planozygote. Encystment of the planozygote into the non-motile non-dividing hypnozygote, (resting cyst) can occur either in the water column, at which the hypnozygotes then fall to the sediment, or after the planozygote actively settles on bottom sediments (Brosnahan et al. 2017). Dormant hypnozygotic organic-walled cyst formation occurs in around 15% dinoflagellates (Head 1996).

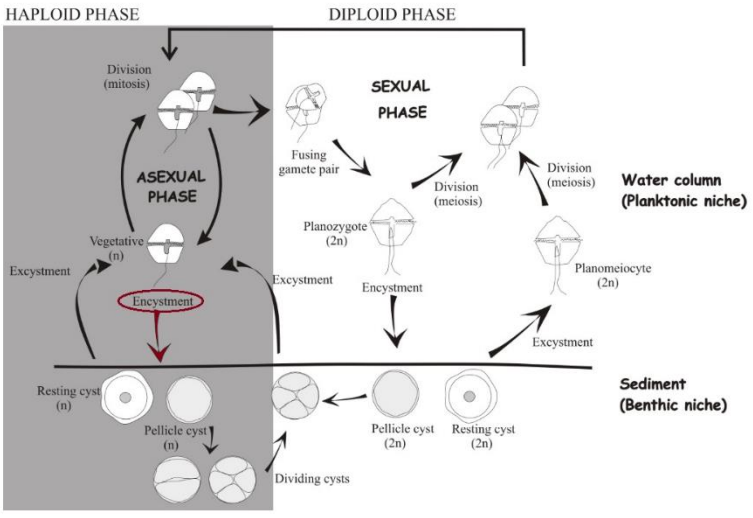

SM: Figure 18 | A dinoflagellate life cycle, including both asexual and sexual origins of cysts. Haploid phase encystment is indicated with a red circle and red arrow. Modified from (Bravo and Figueroa 2014)

References

Álvarez, G., Uribe, E., Díaz, R., Braun, M., Mariño, C. and Blanco, J. 2011. Bloom of the Yessotoxin producing dinoflagellate Protoceratium reticulatum (Dinophyceae) in Northern Chile. *Journal of Sea Research* 65(4), pp. 427–434. Available at: http://dx.doi.org/10.1016/j.seares.2011.03.008.

Anagnostou, E. et al. 2016. Changing atmospheric CO2 concentration was the primary driver of early Cenozoic climate. *Nature* 533, pp. 380–384. doi: 10.1038/nature17423.

Anderson, D.M., Cembella, A.D. and Hallegraeff, G.M. 2012. Progress in understanding harmful algal blooms: Paradigm shifts and new technologies for research, monitoring, and management. *Annual Review of Marine Science* 4, pp. 143–176. doi: 10.1146/annurev-marine-120308-081121.

Anderson, D.M. and Lindquist, N.L. 1985. Time-course measurements of phosphorus depletion and cyst formation in the dinoflagellate Gonyaulax tamarensis Lebour. *Journal of Experimental Marine Biology and Ecology* 86(1), pp. 1–13. doi: 10.1016/0022-0981(85)90039-5.

Badger, M.P.S. 2020. Alkenone isotopes show evidence of active carbon concentrating mechanisms in coccolithophores as aqueous carbon dioxide concentrations fall below 7 µmolL-1. 2(October), pp. 1–19. doi: 10.31223/osf.io/3ywqd.

Badger, M.R., Andrews, T.J., Whitney, S.M., Ludwig, M., Yellowlees, D., Leggat, W. and Price, G.D. 1998. The diversity and coevolution of Rubisco, plastids, pyrenoids, and chloroplast-based CO2-concentrating mechanisms in algae. *Canadian Journal of Botany* 76(6), pp. 1052–1071.

Behrenfeld, M.J. et al. 2006. Climate-driven trends in contemporary ocean productivity. *Nature* 444(7120), pp. 752–755. doi: 10.1038/nature05317.

Berdalet, E., Peters, F., Koumandou, V.L., Roldán, C., Guadayol, Ò. and Estrada, M. 2007. Species-specific physiological response of dinoflagellates to quantified small-scale turbulence. *Journal of Phycology* 43(5), pp. 965–977. doi: 10.1111/j.1529-8817.2007.00392.x.

Berner, R.A. 2006. GEOCARBSULF: A combined model for Phanerozoic atmospheric O2 and CO2. *Geochimica et Cosmochimica Acta* 70(23 SPEC. ISS.), pp. 5653–5664. doi: 10.1016/j.gca.2005.11.032.

Bijl, P.K. et al. 2010. Transient middle eocene atmospheric CO2 and temperature variations. *Science* 330(6005), pp. 819–821. doi: 10.1126/science.1193654.

Black, K.D. 2001. *Environmental Impacts of Aquaculture*. Academic Press, Shellfield.

Blackburn, S.I., Bolch, C.J.S., Haskard, K.A. and Hallegraeff, G.M. 2001. Reproductive compatibility among four global populations of the toxic dinoflagellate Gymnodinium catenatum (Dinophyceae). *Phycologia* 40(1), pp. 78–87. doi: 10.2216/i0031-8884-40-1-78.1.

Bolton, C.T. and Stoll, H.M. 2013. Late Miocene threshold response of marine algae to carbon dioxide limitation. *Nature* 500(7464), pp. 558–562. doi: 10.1038/nature12448.

Boni, L., Ceredi, A., Guerrini, F., Milandri, A., Pistocchi, R., Poletti, R. and Pompei, M. 2001. Toxic Protoceratium reticulatum (Peridinales, Dinophyta) in the North-Western Adriatic Sea (Italy). In: Hallegraeff, G. M., Blackburn, S. I., Bolch, C. J. S., and Lewis, R. J. eds. *Harmful Algal Blooms*. Intergovernmental Oceanographica Commission of UNESCO, Paris, pp. 37–40.

Brading, P., Warner, M.E., Smith, D.J. and Suggett, D.J. 2013. Contrasting modes of inorganic carbon acquisition amongst

Symbiodinium (Dinophyceae) phylotypes. *New Phytologist* 200(2), pp. 432–442. doi: 10.1111/nph.12379.

Brandenburg, K.M. et al. 2017. Combined physical, chemical and biological factors shape Alexandrium ostenfeldii blooms in the Netherlands. *Harmful Algae* 63, pp. 146–153. Available at: http://dx.doi.org/10.1016/j.hal.2017.02.004.

Brandenburg, K.M., Krock, B., Klip, H.C.L., Sluijs, A., Garbeva, P. and Van de Waal, D.B. 2021. Intraspecific variation in multiple trait responses of Alexandrium ostenfeldii towards elevated pCO2. *Harmful Algae* 101(July 2020), p. 101970. doi: 10.1016/j.hal.2020.101970.

Brosnahan, M.L., Fischer, A.D., Lopez, C.B., Moore, S.K. and Anderson, D.M. 2020. Cyst-forming dinoflagellates in a warming climate. *Harmful Algae* 91(December). doi: 10.1016/j.hal.2019.101728.

Brosnahan, M.L., Ralston, D.K., Fischer, A.D., Solow, A.R. and Anderson, D.M. 2017. Bloom termination of the toxic dinoflagellate Alexandrium catenella: Vertical migration behavior, sediment infiltration, and benthic cyst yield. *Limnology and Oceanography* 62(6), pp. 2829–2849. doi: 10.1002/lno.10664.

Van Der Burgh, J., Visscher, H., Dilcher, D.L. and Kürschner, W.M. 1993. Palaeoatmospheric signatures in Neogene fossil leaves. *Science* 260(5115), pp. 1788–1790. doi: 10.1126/science.260.5115.1788.

Burkhardt, S., Riebesell, U. and Zondervan, I. 1999a. Effects of growth rate, CO 2 concentration, and cell size on the stable carbon isotope fractionation in marine phytoplankton. *Geochimica et Cosmochimica Acta* 63(22), pp. 3729–3741.

Burkhardt, S., Riebesell, U. and Zondervan, I. 1999b. Stable carbon isotope fractionation by marine phytoplankton in response to daylength, growth rate, and CO2 availability. 184, pp. 31–41.

Burkholder, J.A.M., Glibert, P.M. and Skelton, H.M. 2008. Mixotrophy, a major mode of nutrition for harmful algal species in eutrophic waters. *Harmful Algae* 8(1), pp. 77–93. doi: 10.1016/j.hal.2008.08.010.

Butler, J.N. 1982. *Carbon dioxide equilibria and their applications*. Addison-Wesley Publishing Company.

Caldeira, K. and Wickett, M. 2003. Anthropogenic carbon and ocean pH. *Nature* 425(September), p. 2003.

Choi, C.J., Brosnahan, M.L., Sehein, T.R., Anderson, D.M. and Erdner, D.L. 2017. Insights into the loss factors of phytoplankton blooms: The role of cell mortality in the decline of two inshore Alexandrium blooms. *Limnology and Oceanography* 62(4), pp. 1742–1753. doi: 10.1002/lno.10530.

Climate Change 2014 Synthesis Report IPCC 2014. *Climate Change 2014 Synthesis Report Summary Chapter for Policymakers*.

Costa, P.R. 2016. Impact and effects of paralytic shellfish poisoning toxins derived from harmful algal blooms to marine fish. *Fish and Fisheries* 17(1), pp. 226–248. doi: 10.1111/faf.12105.

Dagenais-Bellefeuille, S. and Morse, D. 2013. Putting the N in dinoflagellates. *Frontiers in Microbiology* 4(DEC), pp. 1–14. doi: 10.3389/fmicb.2013.00369.

Degens, E.T., Behrendt, M., Gotthardt, B. and Reppmann, E. 1968. Metabolic fractionation of carbon isotopes in marine plankton-II. Data on samples collected off the coasts of Peru and Ecuador. *Deep-Sea Research and Oceanographic Abstracts* 15(1), pp. 11–20. doi: 10.1016/0011-7471(68)90025-9.

Dickson, A.G. and Millero, F.J. 1987. A comparison of the equilibrium constants for the dissociation of carbonic acid in seawater media. *Deep Sea Research Part A, Oceanographic Research Papers* 34(10), pp. 1733–1743. doi: 10.1016/0198-0149(87)90021-5.

Doney, S.C., Fabry, V.J., Feely, R.A. and Kleypas, J.A. 2009. Ocean acidification: The other CO2 problem. *Annual Review of Marine Science* 1, pp. 169–192. doi: 10.1146/annurev.marine.010908.163834.

Doney, S.C. and Schimel, D.S. 2007. Carbon and climate system coupling on timescales from the precambrian to the anthropocene. *Annual Review of Environment and Resources* 32, pp. 31–66. doi: 10.1146/annurev.energy.32.041706.124700.

Dortch, Q., Clayton, J.R., Thoresen, S.S. and Ahmed, S.I. 1984. Species differences in accumulation of nitrogen pools in phytoplankton. *Marine Biology* 81(3), pp. 237–250. doi: 10.1007/BF00393218.

Dunkley Jones, T., Lunt, D.J., Schmidt, D.N., Ridgwell, A., Sluijs, A., Valdes, P.J. and Maslin, M. 2013. Climate model and proxy data constraints on ocean warming across the Palaeocene-Eocene Thermal Maximum. *Earth-Science Reviews* 125, pp. 123–145. Available at: http://dx.doi.org/10.1016/j.earscirev.2013.07.004.

Dyhrman, S.T., Webb, E.A., Anderson, D.M., Moffett, J.W. and Waterbury, J.B. 2002. Cell-specific detection of phosphorus stress in Trichodesmium from the Western North Atlantic. *Limnology and Oceanography* 47(6), pp. 1832–1836. doi: 10.4319/lo.2002.47.6.1832.

Edwards, L.E. 2012. Dinocyst taphonomy, impact craters, cyst ghosts and the Palaeocene-Eocene thermal maximum (PETM). *Palynology* 36(SUPPL. 1), pp. 80–95. doi: 10.1080/01916122.2012.679205.

Eiki, K., Satake, M., Koike, K., Ogata, T., Mitsuya, T. and Oshima, Y. 2005. Confirmation of yessotoxin production by the dinoflagellate Protoceratium reticulatum in Mutsu Bay. *Fisheries Science* 71(3), pp. 633–638. doi: 10.1111/j.1444-2906.2005.01009.x.

Etheridge, D., Steele, L., Langenfels, R., Francey, R., Barnola, J. and Morgan, V. 1998. Historical CO2 record from the Law Done DE08, DE08-2, and DSS ice cores.

Falkowski, P. et al. 2000. The global carbon cycle: A test of our knowledge of earth as a system. *Science* 290(5490), pp. 291–296. doi: 10.1126/science.290.5490.291.

Farquhar, G.D., Ehleringer, J.R. and Hubick, K.T. 1989. Carbon isotope discrimination and photosynthesis. *Annual Review of Plant Physiology and Plant Molecular Biology* 40, pp. 503–537.

Farquhar, G.D., O'Leary, M.H.B. and Berry, J.A. 1982. On the relationship between carbon isotope discrimination and the intercellular carbon dioxide concentration in leaves. *Australian Journal of Plant Physiology* 9, pp. 121–137.

Fensome, A.R.A., MacRae, R.A., Moldowan, J.M., Taylor, F.J.R. and Williams, G.L. 1996. The Early Mesozoic Radiation of Dinoflagellates. *Palaeobiology* 22(3), pp. 329–338.

Field, C.B., Behrenfeld, M.J., Randerson, J.T. and Falkowski, P. 1998. Primary production of the biosphere: Integrating terrestrial and oceanic components. *Science* 281(5374), pp. 237–240. doi: 10.1126/science.281.5374.237.

Finkel, Z. V., Beardall, J., Flynn, K.J., Quigg, A., Rees, T.A. V. and Raven, J.A. 2010. Phytoplankton in a changing world: Cell size and elemental stoichiometry. *Journal of Plankton Research* 32(1), pp. 119–137. doi: 10.1093/plankt/fbp098.

Flynn, K.J. 1991. Algal carbon–nitrogen metabolism: a biochemical basis for modelling the interactions between nitrate and ammonium uptake. *Journal of Plankton Research* 13(2), pp. 373–387.

Foster, G.L. 2008. Seawater pH, pCO2 and [CO2-3] variations in the Caribbean Sea over the last 130 kyr: A boron isotope and B/Ca study of planktic foraminifera. *Earth and Planetary Science Letters* 271(1–4), pp. 254–266. doi: 10.1016/j.epsl.2008.04.015.

Foster, G.L., Lear, C.H. and Rae, J.W.B. 2012. The evolution of pCO 2, ice volume and climate during the middle Miocene. *Earth and Planetary Science Letters* 341–344, pp. 243–254. Available at: http://dx.doi.org/10.1016/j.epsl.2012.06.007.

Freeman, H. and Hayes, J.M. 1992. Fractionation of carbon isotopes by phytoplankton and estimates of ancient CO2 levels. *Global Biogeochemical Cycles* 6(2), pp. 185–198.

Freeman, K.H. and Hayes, J.M. 1990. Evidence from carbon isotope measurements for diverse origins. *Nature* 343(January), pp. 1–18.

Friedlingstein, P. et al. 2019. Global Carbon Budget 2019., pp. 1783–1838.

Friedlingstein, P. et al. 2020. Global Carbon Budget 2020. *Earth System Science Data* 12, pp. 3269–3340.

Frieling, J. et al. 2017. Extreme warmth and heat-stressed plankton in the tropics during the Palaeocene-Eocene Thermal Maximum. *Science Advances* 3(3). doi: 10.1126/sciadv.1600891.

Fu, F.X., Zhang, Y., Warner, M.E., Feng, Y., Sun, J. and Hutchins, D.A. 2008. A comparison of future increased CO2 and temperature effects on sympatric Heterosigma akashiwo and Prorocentrum minimum. *Harmful Algae* 7(1), pp. 76–90. doi: 10.1016/j.hal.2007.05.006.

Fuentes-Grünewald, C., Garcés, E., Alacid, E., Sampedro, N., Rossi, S. and Camp, J. 2012. Improvement of lipid production in the marine strains Alexandrium minutum and Heterosigma akashiwo by utilizing abiotic parameters. *Journal of Industrial Microbiology and Biotechnology* 39(1), pp. 207–216. doi: 10.1007/s10295-011-1016-6.

Fukuda, Y. and Endoh, H. 2006. New details from the complete life cycle of the red-tide dinoflagellate Noctiluca scintillans (Ehrenberg) McCartney. *European Journal of Protistology* 42(3), pp. 209–219. doi: 10.1016/j.ejop.2006.05.003.

García Camacho, F., Gallardo Rodríguez, J.J., Sánchez Mirón, A., Cerón García, M.C., Belarbi, E.H. and Molina Grima, E. 2007. Determination of shear stress thresholds in toxic dinoflagellates cultured in shaken flasks. Implications in bioprocess engineering. *Process Biochemistry* 42(11), pp. 1506–1515. doi: 10.1016/j.procbio.2007.08.001.

Geider, R.J. and La Roche, J. 2002. Redfield revisited: Variability of C:N:P in marine microalgae and its biochemical basis. *European Journal of Phycology* 37(1), pp. 1–17. doi: 10.1017/S0967026201003456.

Giordano, M., Beardall, J. and Raven, J.A. 2005. CO2 concentrating mechanisms in algae: Mechanisms, environmental modulation, and evolution. *Annual Review of Plant Biology* 56, pp. 99–131. doi: 10.1146/annurev.arplant.56.032604.144052.

Gittings, J.A., Raitsos, D.E., Krokos, G. and Hoteit, I. 2018. Impacts of warming on phytoplankton abundance and phenology in a typical tropical marine ecosystem. *Scientific Reports* 8(1), pp. 1–12. Available at: http://dx.doi.org/10.1038/s41598-018-20560-5.

Glibert, P.M., Middelburg, J.J., McClelland, J.W. and Jake Vander Zanden, M. 2019. Stable isotope tracers: Enriching our perspectives and questions on sources, fates, rates, and pathways of major elements in aquatic systems. *Limnology and Oceanography* 64(3), pp. 950–981. doi: 10.1002/lno.11087.

Goericke, R., Montoya, J. and Fry, B. 1994. Physiology of isotopic fractionation in algae and cyanobacteria. In: Lajtha, K. and Michener, R. eds. *Stable Isotopes in Ecology and Environmental Science*. Oxford: Blackwell Scientific Publications, pp. 187–221.

Graneli, E. and Flynn, K. 2006. Chemical and physical factors inflencing toxin content. In: Graneli, E. and Turner, J. T. eds. *Ecology of Harmful Algae*. 189th ed. Springer Berlin Heidelberg, pp. 229–242.

Gruber, N. 2011. Warming up, turning sour, losing breath: Ocean biogeochemistry under global change. *Philosophical Transactions of the Royal Society A: Mathematical, Physical and Engineering Sciences* 369(1943), pp. 1980–1996. doi: 10.1098/rsta.2011.0003.

Guerrini, F., Ciminiello, P., Dell'Aversano, C., Tartaglione, L., Fattorusso, E., Boni, L. and Pistocchi, R. 2007. Influence of temperature, salinity and nutrient limitation on yessotoxin production and release by the dinoflagellate Protoceratium reticulatum in batch-cultures. *Harmful Algae* 6(5), pp. 707–717. doi: 10.1016/j.hal.2007.02.006.

Guillard, R.R.L. and Ryther, J.H. 1962. Studies of marine planktonic diatoms. I. Cyclotella nana Hustedt and Detonula confervacea (Cleve) Gran. *Canadian Journal of Microbiology* 8, pp. 229–239.

Hallegraeff, G.M. 2010. Ocean climate change, phytoplankton community responses, and harmful algal blooms: A formidable predictive challenge. *Journal of Phycology* 46(2), pp. 220–235. doi: 10.1111/j.1529-8817.2010.00815.x.

Hansen, P.J. 2002. Effect of high pH on the growth and survival of marine phytoplankton: implications for species succession. 28, pp. 279–288.

Hansen, P.J., Lundholm, N. and Rost, B. 2007. Growth limitation in marine red-tide dinoflagellates: Effects of pH versus inorganic carbon availability. *Marine Ecology Progress Series* 334, pp. 63–71. doi: 10.3354/meps334063.

Hayes, J.M., Freeman, K.H., Popp, B.N. and Hoham, C.H. 1990. Compound-specific isotopic analyses: A novel tool for reconstruction of ancient biogeochemical processes. 16, pp. 1115–1128. Available at: papers://d389027f-1c90-43ee-8f36-77ce4678000f/Paper/p85.

Hays, J.D., Imbrie, J. and Shackleton, N.J. 1976. Variations in the Earth's Orbit : Pacemaker of the Ice Ages. *Science* 194(4270), pp. 1121–1132.

Head, M.J. 1996. Modern dinoflagellate cysts and their biological affinities. In: Jansonius, J. and McGregor, D. C. eds. *Palynology: Principles and Applications*. Dallas, pp. 1197–1248.

Hennon, G.M.M. et al. 2015. Diatom acclimation to elevated CO2 via cAMP signalling and coordinated gene expression. *Nature Climate Change* 5, pp. 761–765.

Hernández-Becerril, D.U. et al. 2007. Toxic and harmful marine phytoplankton and microalgae (HABs) in Mexican Coasts. *Journal of Environmental Science and Health - Part A Toxic/Hazardous Substances and Environmental Engineering* 42(10), pp. 1349–1363. doi: 10.1080/10934520701480219.

Heureux, A.M.C. and Rickaby, R.E.M. 2015. Refining our estimate of atmospheric CO2 across the eocene-Oligocene climatic transition. *Earth and Planetary Science Letters* 409, pp. 329–338. Available at: http://dx.doi.org/10.1016/j.epsl.2014.10.036.

Hinga, K.R., Arthur, M.A., Pilson, M.E.Q. and Whitaker, D. 1994. Carbon isotope fractionation by marine phytoplankton in culture: The effects of CO2 concentration, pH, temperature, and species. *Global Biogeochemical Cycles* 8(1), pp. 91–102. doi: 10.1029/93GB03393.

Hoins, M. et al. 2016a. Combined effects of ocean acidification and light or nitrogen availabilities on 13C fractionation in marine dinoflagellates. *PLoS ONE* 11(5), pp. 1–16. doi: 10.1371/journal.pone.0154370.

Hoins, M., Eberlein, T., Van de Waal, D.B., Sluijs, A., Reichart, G.J. and Rost, B. 2016b. CO2-dependent carbon isotope fractionation in dinoflagellates relates to their inorganic carbon fluxes. *Journal of Experimental Marine Biology and Ecology* 481, pp. 9–14. doi: 10.1016/j.jembe.2016.04.001.

Hoins, M., Van de Waal, D.B., Eberlein, T., Reichart, G.J., Rost, B. and Sluijs, A. 2015. Stable carbon isotope fractionation of organic cyst-forming dinoflagellates: Evaluating the potential for a CO2 proxy. *Geochimica et Cosmochimica Acta* 160, pp. 267–276. doi: 10.1016/j.gca.2015.04.001.

Hönisch, B., Hemming, N.G., Archer, D., Siddall, M. and McManus, J.F. 2019. Atmospheric carbon dioxide concentration across the Mid-Pleistocene Transition. *Science* 234, pp. 1551–1555. doi: 10.7551/mitpress/8876.003.0036.

Hurd, C.L. et al. 2020. Ocean acidification as a multiple driver: How interactions between changing seawater carbonate parameters affect marine life. *Marine and Freshwater Research* 71(3), pp. 263–274. doi: 10.1071/MF19267.

Ingarao, C., Ricci, F., Carlo, U. and Carlo, U. 2006. Distribution of phytoplanktonic populations (Bacillariophyceae and

Dinophyceae) along the ... (January)

IPCC 2019. The Ocean and Cryosphere in a Changing Climate. A Special Report of the Intergovernmental Panel on Climate Change. *Intergovernmental Panel on Climate Change* , pp. 1–765. Available at: https://www.ipcc.ch/srocc/chapter/summary-for-policymakers/.

Jansson, I.M. et al. 2014. Statistically assessing the correlation between salinity and morphology in cysts produced by the dinoflagellate Protoceratium reticulatum from surface sediments of the North Atlantic Ocean, Mediterranean-Marmara-Black Sea region, and Baltic-Kattegat-Skage. *Palaeogeography, Palaeoclimatology, Palaeoecology* 399, pp. 202–213. Available at: http://dx.doi.org/10.1016/j.palaeo.2014.01.012.

Jasper, J.P. and Hayes, J.M. 1990. A carbon isotope record of CO2 levels during the late Quaternary. *Nature* 347(6292), pp. 462–464. doi: 10.1038/347462a0.

Jouzel, J. et al. 2007. Orbital and Millennial Antarctic Climate Variability over the Past 800,000 Years. *Science* 317(5839), pp. 793–796.

Keeling, C.D. 1960. The Concentration and Isotopic Abundances of Carbon Dioxide in the Atmosphere. *Tellus* 12(2), pp. 200–203. doi: 10.3402/tellusa.v12i2.9366.

Keller, M.D., Selvin, R.C., Calus, W. and Guillard, R.R.L. 1987. Media for the culture of oceanic ultraphytoplankton. *Journal of Phycology* 23(4), pp. 633–638.

Klais, R., Tamminen, T., Kremp, A., Spilling, K., An, B.W., Hajdu, S. and Olli, K. 2013. Spring phytoplankton communities shaped by interannual weather variability and dispersal limitation: Mechanisms of climate change effects on key coastal primary producers. *Limnology and Oceanography* 58(2), pp. 753–762. doi: 10.4319/lo.2013.58.2.0753.

Klais, R., Tamminen, T., Kremp, A., Spilling, K. and Olli, K. 2011. Decadal-scale changes of Dinoflagellates and Diatoms in the Anomalous Baltic Sea spring bloom. *PLoS ONE* 6(6). doi: 10.1371/journal.pone.0021567.

Koike, K. et al. 2006. Protoceratium reticulatum in northern Japan: Environmental factors associated with seasonal occurrence and related contamination of yessotoxin in scallops. *Journal of Plankton Research* 28(1), pp. 103–112. doi: 10.1093/plankt/fbi103.

Kremp, A., Godhe, A., Egardt, J., Dupont, S., Suikkanen, S., Casabianca, S. and Penna, A. 2012. Intraspecific variability in the response of bloom-forming marine microalgae to changed climate conditions. *Ecology and Evolution* 2(6), pp. 1195–1207. doi: 10.1002/ece3.245.

Kürschner, W.M., Kvaček, Z. and Dilcher, D.L. 2008. The impact of Miocene atmospheric carbon dioxide fluctuations on climate and the evolution of terrestrial ecosystems. *Proceedings of the National Academy of Sciences of the United States of America* 105(2), pp. 449–453. doi: 10.1073/pnas.0708588105.

Laws, E.A., Bidigare, R.R. and Popp, B.N. 1997. Effect of growth rate and CO2 concentration on carbon isotopic fractionation by the marine diatom Phaeodactylum tricornutum. *Limnology and Oceanography* 42(7), pp. 1552–1560. doi: 10.4319/lo.1997.42.7.1552.

Laws, E.A., Popp, B.N., Bidigare, R.R., Kennicutt, M.C. and Macko, S.A. 1995. Dependence of phytoplankton carbon isotopic composition on growth rate and [CO2)aq: Theoretical considerations and experimental results. *Geochimica et Cosmochimica Acta* 59(6), pp. 1131–1138. doi: 10.1016/0016-7037(95)00030-4.

Laws, E.A., Popp, B.N., Cassar, N. and Tanimoto, J. 2002. 13C discrimination patterns in oceanic phytoplankton: Likely influence of CO2 concentrating mechanisms, and implications for palaeoreconstructions. *Functional Plant Biology* 29(2–3), pp. 323–333. doi: 10.1071/pp01183.

Lee, K.H. et al. 2016. Mixotrophic ability of the phototrophic dinoflagellates Alexandrium andersonii, A. affine, and A. fraterculus. *Harmful Algae* 59, pp. 67–81. doi: 10.1016/j.hal.2016.09.008.

Lei, Q.Y. and Lu, S.H. 2011. Molecular ecological responses of the dinoflagellate Karenia mikimotoi to phosphate stress. *Harmful Algae* 12, pp. 39–45. Available at: http://dx.doi.org/10.1016/j.hal.2011.08.010.

Leong, S.C.Y. and Taguchi, S. 2004. Response of the dinoflagellate Alexandrium tamarense to a range of nitrogen sources and concentrations: Growth rate, chemical carbon and nitrogen, and pigments. *Hydrobiologia* 515, pp. 215–224. doi: 10.1023/B:HYDR.0000027331.49819.a4.

Li, G., Cheng, L., Zhu, J., Trenberth, K.E., Mann, M.E. and Abraham, J.P. 2020. Increasing ocean stratification over the past half-century. *Nature Climate Change* 10(12), pp. 1116–1123. Available at: http://dx.doi.org/10.1038/s41558-020-00918-2.

Li, M., Shi, X., Guo, C. and Lin, S. 2016. Phosphorus deficiency inhibits cell division but not growth in the dinoflagellate Amphidinium carterae. *Frontiers in Microbiology* 7(JUN), pp. 1–11. doi: 10.3389/fmicb.2016.00826.

Lilley, R.M., Ralph, P.J. and Larkum, A.W.D. 2010. The determination of activity of the enzyme Rubisco in cell extracts of the dinoflagellate alga Symbiodinium sp. by manganese chemiluminescence and its response to short-term thermal stress of the alga. *Plant, Cell and Environment* 33(6), pp. 995–1004. doi: 10.1111/j.1365-3040.2010.02121.x.

Litchman, E., Klausmeier, C.A., Schofield, O.M. and Falkowski, P.G. 2007. The role of functional traits and trade-offs in structuring phytoplankton communities: Scaling from cellular to ecosystem level. *Ecology Letters* 10(12), pp. 1170–1181. doi: 10.1111/j.1461-0248.2007.01117.x.

Lomas, M.W., Swain, A., Shelton, R. and Ammerman, J.W. 2004. Taxonomic variability of phosphorus stress in Sargasso Sea phytoplankton. *Limnology and Oceanography* 49(6), pp. 2303–2309. doi: 10.4319/lo.2004.49.6.2303.

Lüthi, D. et al. 2008. High-resolution carbon dioxide concentration record 650,000-800,000 years before present. *Nature* 453(7193), pp. 379–382. doi: 10.1038/nature06949.

Mantle, D.J., Riding, J.B. and Hannaford, C. 2020. Late Triassic dinoflagellate cysts from the Northern Carnarvon Basin, Western Australia. *Review of Palaeobotany and Palynology* 281, p. 104254. Available at: https://doi.org/10.1016/j.revpalbo.2020.104254.

Marret, F. and Zonneveld, K.A.F. 2003. Atlas of modern organic-walled dinoflagellate cyst distribution. *Review of Palaeobotany and Palynology* 125(1–2), pp. 1–200. doi: 10.1016/S0034-6667(02)00229-4.

Matsumoto, K., Tanioka, T. and Rickaby, R. 2020. Linkages between dynamic phytoplankton c:N:P and the ocean carbon cycle under climate change. *Oceanography* 33(2), pp. 44–52. doi: 10.5670/oceanog.2020.203.

Mehrbach, C., Culberson, C.H., Hawley, J.E. and Pytkowicx, R.M. 1973. Measurement of the Apparent Dissociation Constants of Carbonic Acid in Seawater At Atmospheric Pressure. *Limnology and Oceanography* 18(6), pp. 897–907. doi: 10.4319/lo.1973.18.6.0897.

Meinshausen, M. et al. 2011. The RCP greenhouse gas concentrations and their extensions from 1765 to 2300. *Climatic Change* 109(1), pp. 213–241. doi: 10.1007/s10584-011-0156-z.

Mertens, K.N., Dale, B., Ellegaard, M., Jansson, I.M., Godhe, A., Kremp, A. and Louwye, S. 2011. Process length variation in cysts of the dinoflagellate Protoceratium reticulatum, from surface sediments of the Baltic-Kattegat-Skagerrak estuarine system: A regional salinity proxy. *Boreas* 40(2), pp. 242–255. doi: 10.1111/j.1502-3885.2010.00193.x.

Middelburg, J.J. 2019. *Marine Carbon Biogeochemistry: A Primer for Earth System Scientists*. Available at: http://www.springer.com/series/10032%0Ahttp://link.springer.com/10.1007/978-3-030-10822-9.

Mitra, A. et al. 2016. Defining Planktonic Protist Functional Groups on Mechanisms for Energy and Nutrient Acquisition:

Incorporation of Diverse Mixotrophic Strategies. *Protist* 167(2), pp. 106–120. Available at: http://dx.doi.org/10.1016/j.protis.2016.01.003.

Monnin, E. et al. 2001. Atmospheric CO2 concentrations over the last glacial termination. *Science* 291(5501), pp. 112–114. doi: 10.1126/science.291.5501.112.

Montechiaro, F. and Giordano, M. 2010. Compositional homeostasis of the dinoflagellate Protoceratium reticulatum grown at three different pCO2. *Journal of Plant Physiology* 167(2), pp. 110–113. Available at: http://dx.doi.org/10.1016/j.jplph.2009.07.013.

Mook, W.G., Bommerson, J.C. and Staverman, W.H. 1974. Carbon isotope fractionation between dissolved bicarbonate and gaseous carbon dioxide. *Earth and Planetary Science Letters* 22(2), pp. 169–176. doi: 10.1016/0012-821X(74)90078-8.

Moore, C.M., Mills, M.M., Langlois, R., Milne, A., Achterberg, E.P., La Roche, J. and Geider, R.J. 2008. Relative influence of nitrogen and phosphorus availability on phytoplankton physiology and productivity in the oligotrophic sub-tropical North Atlantic Ocean. *Limnology and Oceanography* 53(1), pp. 291–305. doi: 10.4319/lo.2008.53.1.0291.

Moore, S.K., Mantua, N.J. and Salathé, E.P. 2011. Past trends and future scenarios for environmental conditions favoring the accumulation of paralytic shellfish toxins in Puget Sound shellfish. *Harmful Algae* 10(5), pp. 521–529. doi: 10.1016/j.hal.2011.04.004.

Van Mooy, B.A.S. et al. 2009. Phytoplankton in the ocean use non-phosphorus lipids in response to phosphorus scarcity. *Nature* 458(7234), pp. 69–72. doi: 10.1038/nature07659.

Morquecho, L. 2019. Pyrodinium bahamense one the most significant harmful dinoflagellate in Mexico. *Frontiers in Marine Science* 6(JAN). doi: 10.3389/fmars.2019.00001.

Morse, D., Salois, P., Markovic, P. and Hastings, J.W. 1995. A Nuclear-Encoded Form II RuBisCO in Dinoflagellates. *Science* 268(5217), pp. 1622–1624.

Ni, Y. et al. 2007. A core top assessment of proxies for the ocean carbonate system in surface-dwelling foraminifers. *Palaeoceanography* 22(3). doi: 10.1029/2006PA001337.

NOAA 2021. Global Monthly Mean CO2. Available at: https://www.esrl.noaa.gov/gmd/ccgg/trends/global.html [Accessed: 6 March 2021].

Olli, K. and Anderson, D.M. 2002. High encystment success of the dinoflagellate Scrippsiella cf. lachrymosa in culture experiments. *Journal of Phycology* 38(1), pp. 145–156. doi: 10.1046/j.1529-8817.2002.01113.x.

Pagani, M. 2014. *Biomarker-Based Inferences of Past Climate: The Alkenone pCO2 Proxy*. 2nd ed. Elsevier Ltd. Available at: http://dx.doi.org/10.1016/B978-0-08-095975-7.01027-5.

Pardue, J.W., Scalan, R.S., Van Baalen, C. and Parker, P.L. 1976. Maximum carbon isotope fractionation in photosynthesis by blue-green algae and a green alga. *Geochimica et Cosmochimica Acta* 40(3), pp. 309–312. doi: 10.1016/0016-7037(76)90208-8.

Paz, B. 2008. Yessotoxins, a Group of Marine Polyether Toxins: an Overview. *Marine Drugs* 6(2), pp. 73–102. doi: 10.3390/md20080005.

Paz, B., Riobó, P., Luisa Fernández, M., Fraga, S. and Franco, J.M. 2004. Production and release of yessotoxins by the dinoflagellates Protoceratium reticulatum and Lingulodinium polyedrum in culture. *Toxicon* 44(3), pp. 251–258. doi: 10.1016/j.toxicon.2004.05.021.

Pearson, P.N., Foster, G.L. and Wade, B.S. 2009. Atmospheric carbon dioxide through the Eocene-Oligocene climate transition. *Nature* 461(7267), pp. 1110–1113. doi: 10.1038/nature08447.

Peperzak, L. 2003. Climate change and harmful algal blooms in the North Sea. *Acta Oecologica* 24(SUPPL. 1). doi: 10.1016/S1146-609X(03)00009-2.

Petit, J.R. et al. 2013. Climate and atmospheric history of the past 420,000 years from the Vostok ice core, Antarctica. *The Future of Nature: Documents of Global Change* , pp. 348–358.

Pfiester, L.A. and Anderson, D.M. 1987. Dinoflagellate reproduction. In: *The Biology of Dinoflagellates*.

Pierangelini, M., Raven, J.A. and Giordano, M. 2017. The relative availability of inorganic carbon and inorganic nitrogen influences the response of the dinoflagellate Protoceratium reticulatum to elevated CO2. *Journal of Phycology* 53(2), pp. 298–307. doi: 10.1111/jpy.12463.

Pierce, R.H. and Henry, M.S. 2008. Harmful algal toxins of the Florida red tide (Karenia brevis): natural chemical stressors in South Florida coastal ecosystems. *Ecotoxicology* 17(7), pp. 623–631. doi: 10.1007/s10646-008-0241-x.Harmful.

Pierrot, D., Lewis, E. and Wallace, D.W.R. 2006. MS excel program developed for CO2 system calculations, ORNL/CDIAC-105a, Carbon Dioxide Information Analysis Center, Oak Ridge National Laboratory, US Department of Energy, Oak Ridge, Tennessee.

Popp, B.N., Laws, E.A., Bidigare, R.R., Dore, J.E., Hanson, K.L. and Wakeham, S.G. 1998. Effect of phytoplankton cell geometry on carbon isotopic fractionation. *Geochimica et Cosmochimica Acta* 62(1), pp. 69–77. doi: 10.1016/S0016-7037(97)00333-5.

Popp, B.N., Parekh, P., Tilbrook, B., Bidigare, R.R. and Laws, E.A. 1997. Organic carbon δ13C variations in sedimentary rocks as chemostratigraphic and palaeoenvironmental tools. *Palaeogeography, Palaeoclimatology, Palaeoecology* 132(1–4), pp. 119–132. doi: 10.1016/S0031-0182(97)00061-8.

Pross, J. and Brinkhuis, H. 2005. Organic-walled dinoflagellate cysts as palaeoenvironmental indicators in the Palaeogene; a synopsis of concepts. *Paläontologische Zeitschrift* 79(1), pp. 53–59. doi: 10.1007/bf03021753.

R Development Core Team 2019. R: A Language and Environment for Statistical Cmputing.

Ratti, S., Giordano, M. and Morse, D. 2007. CO2-concentrating mechanisms of the potentially toxic dinoflagellate Protoceratium reticulatum (Dinophyceae, Gonyaulacales). *Journal of Phycology* 43(4), pp. 693–701. doi: 10.1111/j.1529-8817.2007.00368.x.

Rau, G.H., Takahashi, T. and Des Marais, D.J. 1989. Latitudinal variations in plankton δ13C: Implications for CO2 and productivity in past oceans. *Nature* 341(6242), pp. 516–518. doi: 10.1038/341516a0.

Raven, B.Y.J.A. 1987. THE ROLE OF VACUOLES Department of Biological Sciences , University of Dundee ,.

Raven, J.A. 1997. The Vacuole: A cost-benefit analysis. *Advances in Botanical Research* 25, pp. 59–86.

Raven, J.A., Giordano, M. and Beardall, J. 2008. Insights into the evolution of CCMs from comparisons with other resource acquisition and assimilation processes. *Physiologia Plantarum* 133(1), pp. 4–14. doi: 10.1111/j.1399-3054.2007.01024.x.

Raven, J.A. and Johnston, A. 1991. Mechanisms of inorganic-carbon acquisition in marine phytoplankton and their implications for the use of other resources concentration on growth and photosynthe- sis by marine phytoplankton organisms has been little investigated relative to the effects me. 36

Raymo, M.E., Grant, B., Horowitz, M. and Rau, G.H. 1996. Mid-Pliocene warmth: Stronger greenhouse and stronger conveyor. *Marine Micropalaeontology* 27(1–4), pp. 313–326. doi: 10.1016/0377-8398(95)00048-8.

Rein, K.S. and Borrone, J. 1999. Polyketides from dinoflagellates: Origins, pharmacology and biosynthesis. *Comparative Biochemistry and Physiology - B Biochemistry and Molecular Biology* 124(2), pp. 117–131. doi: 10.1016/S0305-

0491(99)00107-8.

Reinfelder, J.R. 2011. Carbon concentrating mechanisms in eukaryotic marine phytoplankton. *Annual Review of Marine Science* 3, pp. 291–315. doi: 10.1146/annurev-marine-120709-142720.

Rhodes, L., McNabb, P., De Salas, M., Briggs, L., Beuzenberg, V. and Gladstone, M. 2006. Yessotoxin production by Gonyaulax spinifera. *Harmful Algae* 5(2), pp. 148–155. doi: 10.1016/j.hal.2005.06.008.

Ribeiro, S., Berge, T., Lundholm, N., Andersen, T.J., Abrantes, F. and Ellegaard, M. 2011. Phytoplankton growth after a century of dormancy illuminates past resilience to catastrophic darkness. *Nature Communications* 2(1). doi: 10.1038/ncomms1314.

Röder, K. et al. 2012. Effects of salinity, temperature and nutrients on growth, cellular characteristics and yessotoxin production of Protoceratium reticulatum. *Harmful Algae* 15, pp. 59–70. doi: 10.1016/j.hal.2011.11.006.

Rodríguez, J.J.G., Mirón, A.S., Camacho, F.G., García, M.C.C., Belarbi, E.H., Chisti, Y. and Grima, E.M. 2009. Causes of shear sensitivity of the toxic dinoflagellate protoceratium reticulatum. *Biotechnology Progress* 25(3), pp. 792–800. doi: 10.1002/btpr.161.

van Roij, L., Sluijs, A., Laks, J.J. and Reichart, G.J. 2017. Stable carbon isotope analyses of nanogram quantities of particulate organic carbon (pollen) with laser ablation nano combustion gas chromatography/isotope ratio mass spectrometry. *Rapid Communications in Mass Spectrometry* 31(1), pp. 47–58. doi: 10.1002/rcm.7769.

Rossi, S. and Fiorillo, I. 2010. Biochemical features of a protoceratium reticulatum red tide in Chipana Bay (Northern Chile) in summer conditions. *Scientia Marina* 74(4), pp. 633–642. doi: 10.3989/scimar.2010.74n4633.

Rost, B., Richter, K.U., Riebesell, U. and Hansen, P.J. 2006a. Inorganic carbon acquisition in red tide dinoflagellates. *Plant, Cell and Environment* 29(5), pp. 810–822. doi: 10.1111/j.1365-3040.2005.01450.x.

Rost, B., Riebesell, U. and Sültemeyer, D. 2006b. Carbon acquisition of marine phytoplankton: Effect of photoperiod length. *Limnology and Oceanography* 51(1 I), pp. 12–20. doi: 10.4319/lo.2006.51.1.0012.

Rost, B., Zondervan, I. and Riebesell, U. 2002. Light-dependent carbon isotope fractionation in the coccolithophorid Emiliania huxleyi. *Limnology and Oceanography* 47(1), pp. 120–128. doi: 10.4319/lo.2002.47.1.0120.

Rost, B., Zondervan, I. and Wolf-Gladrow, D. 2008. Sensitivity of phytoplankton to future changes in ocean carbonate chemistry: Current knowledge, contradictions and research directions. *Marine Ecology Progress Series* 373, pp. 227–237. doi: 10.3354/meps07776.

Royer, D.L. 2001. Stomatal density and stomatal index as indicators of palaeoatmospheric CO2 concentration. *Review of Palaeobotany and Palynology* 114(1–2), pp. 1–28. doi: 10.1016/S0034-6667(00)00074-9.

Ruddiman, W.F. 2008. *Earth's Climate: Past and Future*. Second Edi. W.H. Freeman and Co.

Sackett, W., Eckelmann, W., Bender, M. and Bé, A.W.H. 1965. Temperature Dependence of Carbon Isotope Composition in Marine Plankton and Sediments Author (s): William M . Published by : American Association for the Advancement of Science Sta. *Science* 148(3667), pp. 235–237.

Sackett, W.M. 1986. δ13C signatures of organic carbon in southern high latitude deep sea sediments; palaeotemperature implications. *Organic Geochemistry* 9(2), pp. 63–68. doi: 10.1016/0146-6380(86)90087-2.

Sala-Pérez, M., Alpermann, T.J., Krock, B. and Tillmann, U. 2016. Growth and bioactive secondary metabolites of arctic Protoceratium reticulatum (Dinophyceae). *Harmful Algae* 55, pp. 85–96. doi: 10.1016/j.hal.2016.02.004.

Sanseverino, I., Conduto, D., Pozzoli, L., Dobricic, S. and Lettieri, T. 2016. *Algal bloom and its economic impact*.

Santos, A., de Araujo Carvalho, M., de Oliveira, A.D. and Mendonça Filho, J.G. 2017. Palaeoenvironmental changes and influence on Operculodinium centrocarpum during the Quaternary in the Campos Basin, southwestern Brazil. *Journal of South American Earth Sciences* 80, pp. 255–271. doi: 10.1016/j.jsames.2017.09.020.

Satake, M., MacKenzie, L. and Yasumoto, T. 1997. Identification of Protoceratium reticulatum as the biogenetic origin of yessotoxin. *Natural Toxins* 5(4), pp. 164–167. doi: 10.1002/19970504nt7.

De Schepper, S., Beck, K.M. and Mangerud, G. 2017. Late Neogene dinoflagellate cyst and acritarch biostratigraphy for Ocean Drilling Program Hole 642B, Norwegian Sea. *Review of Palaeobotany and Palynology* 236, pp. 12–32. Available at: http://dx.doi.org/10.1016/j.revpalbo.2016.08.005.

Sharkey, T.D. and Berry, J.A. 1985. Carbon isotope fractionatino of algae as influenced by an inducible CO2 concentration mechanism. *The american society of plan physiologists* (891), pp. 389–401.

Siegenthaler, U. 2010. Stable Carbon Cycle – Climate Relationship During the Late Pleistocene Stable Carbon Cycle – Climate Relationship During the Late Pleistocene. 1313(NOVEMBER), pp. 1313–1317.

Sigman, D.M. and Boyle, E.A. 2000. Glacial/Interglacial changes in atmospheric carbon dioxide. *Nature* 407(October), pp. 859–869.

Sluijs, A., Pross, J. and Brinkhuis, H. 2005. From greenhouse to icehouse; organic-walled dinoflagellate cysts as palaeoenvironmental indicators in the Palaeogene. *Earth-Science Reviews* 68(3–4), pp. 281–315. doi: 10.1016/j.earscirev.2004.06.001.

Sluijs, A., van Roij, L., Frieling, J., Laks, J. and Reichart, G.J. 2018. Single-species dinoflagellate cyst carbon isotope ecology across the Palaeocene-Eocene Thermal Maximum. *Geology* 46(1), pp. 79–82. doi: 10.1130/G39598.1.

Smayda, T.J. 1997. Harmful algal blooms: Their ecophysiology and general relevance to phytoplankton blooms in the sea. *Limnology and Oceanography* 42(5 II), pp. 1137–1153. doi: 10.4319/lo.1997.42.5_part_2.1137.

Smayda, T.J. and Reynolds, C.S. 2003. Strategies of marine dinoflagellate survival and some rules of assembly. *Journal of Sea Research* 49(2), pp. 95–106. doi: 10.1016/S1385-1101(02)00219-8.

Stoll, H.M. et al. 2019. Upregulation of phytoplankton carbon concentrating mechanisms during low CO 2 glacial periods and implications for the phytoplankton pCO 2 proxy. *Quaternary Science Reviews* 208, pp. 1–20. Available at: https://doi.org/10.1016/j.quascirev.2019.01.012.

Von Stosch, H.A. 1973. Observations on vegetative reproduction and sexual life cycles of two freshwater dinoflagellates, gymno- d ini um pseudopalustre schiller and woloszynskia apiculata sp. Nov. *British Phycological Journal* 8(2), pp. 105–134. doi: 10.1080/00071617300650141.

Tanaka, T. et al. 2011. Lack of P-limitation of phytoplankton and heterotrophic prokaryotes in surface waters of three anticyclonic eddies in the stratified Mediterranean Sea. *Biogeosciences* 8(2), pp. 525–538. doi: 10.5194/bg-8-525-2011.

Tatters, A.O., Flewelling, L.J., Fu, F., Granholm, A.A. and Hutchins, D.A. 2013. High CO2 promotes the production of paralytic shellfish poisoning toxins by Alexandrium catenella from Southern California waters. *Harmful Algae* 30, pp. 37–43. Available at: http://dx.doi.org/10.1016/j.hal.2013.08.007.

Thomas, W.H. and Gibson, C.H. 1990. Effects of small-scale turbulence on microalgae. *Journal of Applied Phycology* 2, pp. 71–77.

Tillmann, U. and Hoppenrath, M. 2013. Life Cycle of the Pseudocolonial Dinoflagellate Polykrikos kofoidii (Gymnodiniales, Dinoflagellata). *Journal of Phycology* 49(2), pp. 298–317. doi: 10.1111/jpy.12037.

Tubaro, A., Dell'Ovo, V., Sosa, S. and Florio, C. 2010. Yessotoxins: A toxicological overview. *Toxicon* 56(2), pp. 163–172.

Available at: http://dx.doi.org/10.1016/j.toxicon.2009.07.038.

Turpin, D.H. 1991. Effects of inorganic N availability on algal photosynthesis and carbon metabolism. *Journal of Phycology* 27(1), pp. 14–20.

Verhoeven, K. and Louwye, S. 2012. Selenopemphix islandensis sp. nov.: A new organic-walled dinoflagellate cyst from the Lower Pliocene Tjörnes beds, northern Iceland. *Palynology* 36(1), pp. 10–25. doi: 10.1080/01916122.2011.593573.

Verleye, T.J. et al. 2012. Average process length variation of the marine dinoflagellate cyst Operculodinium centrocarpum in the tropical and Southern Hemisphere Oceans: Assessing its potential as a palaeosalinity proxy. *Marine Micropalaeontology* 86–87, pp. 45–58. Available at: http://dx.doi.org/10.1016/j.marmicro.2012.02.001.

De Vernal, A., Rochon, A., Turon, J.L. and Matthiessen, J. 1997. Organic-walled dinoflagellate cysts: Palynological tracers of sea-surface conditions in middle to high latitude marine environments. *Geobios* 30(7), pp. 905–920. doi: 10.1016/S0016-6995(97)80215-X.

Verspagen, J.M.H., Van de Waal, D.B., Finke, J.F., Visser, P.M. and Huisman, J. 2014. Contrasting effects of rising CO2 on primary production and ecological stoichiometry at different nutrient levels. *Ecology Letters* 17(8), pp. 951–960. doi: 10.1111/ele.12298.

Versteegh, G.J.M., Blokker, P., Marshall, C. and Pross, J. 2007. Macromolecular composition of the dinoflagellate cyst Thalassiphora pelagica (Oligocene, SW Germany). *Organic Geochemistry* 38(10), pp. 1643–1656. doi: 10.1016/j.orggeochem.2007.06.007.

Van de Waal, D.B., Brandenburg, K.M., Keuskamp, J., Trimborn, S., Rokitta, S., Kranz, S.A. and Rost, B. 2019. Highest plasticity of carbon-concentrating mechanisms in earliest evolved phytoplankton. *Limnology and Oceanography Letters* , pp. 37–43. doi: 10.1002/lol2.10102.

Van De Waal, D.B., Eberlein, T., John, U., Wohlrab, S. and Rost, B. 2014. Impact of elevated pCO2 on paralytic shellfish poisoning toxin content and composition in Alexandrium tamarense. *Toxicon* 78, pp. 58–67. Available at: http://dx.doi.org/10.1016/j.toxicon.2013.11.011.

Van de Waal, D.B., Smith, V.H., Declerck, S.A.J., Stam, E.C.M. and Elser, J.J. 2014. Stoichiometric regulation of phytoplankton toxins. *Ecology Letters* 17(6), pp. 736–742. doi: 10.1111/ele.12280.

Wall, D. and Dale, B. 1966. “Living fossils” in western Atlantic plankton. *Nature* , pp. 1025–1026.

Wall, D., Dale, B., Lohmann, G.P. and Smith, W.K. 1977. The environmental and climatic distribution of dinoflagellate cysts in modern marine sediments from regions in the North and South Atlantic Oceans and adjacent seas. *Marine Micropalaeontology* 2(C), pp. 121–200. doi: 10.1016/0377-8398(77)90008-1.

Wang, Z.H., Qi, Y.Z. and Yang, Y.F. 2007. Cyst formation: An important mechanism for the termination of Scrippsiella trochoidea (Dinophyceae) bloom. *Journal of Plankton Research* 29(2), pp. 209–218. doi: 10.1093/plankt/fbm008.

Wells, M.L. and Karlson, B. 2018. Harmful Algal Blooms in a Changing Ocean., pp. 77–90. doi: 10.1007/978-3-319-70069-4_5.

Whitney, S.M. et al. 1995. Evidence that Some Dinoflagellates Contain a Ribulose-1 , 5-bisphosphate Carboxylase / Oxygenase Related to that of the α -proteobacteria Published by : Royal Society REFERENCES Linked references are available on JSTOR for this article : Evidence that som. 259(1356), pp. 271–275.

Whitney, S.M. and Andrews, T.J. 1998. The CO2/O2 specificity of single-subunit ribulose-bisphosphate carboxylase from the dinoflagellate, Amphidinium carterae. *Australian Journal of Plant Physiology* 25, pp. 131–138.

Wilkes, E.B., Carter, S.J. and Pearson, A. 2017. CO2-dependent carbon isotope fractionation in the dinoflagellate

Alexandrium tamarense. *Geochimica et Cosmochimica Acta* 212, pp. 48–61. Available at: http://dx.doi.org/10.1016/j.gca.2017.05.037.

Wilkes, E.B. and Pearson, A. 2019. A general model for carbon isotopes in red-lineage phytoplankton: Interplay between unidirectional processes and fractionation by RubisCO. *Geochimica et Cosmochimica Acta* 265, pp. 163–181. Available at: https://doi.org/10.1016/j.gca.2019.08.043.

Witkowski, C.R., Weijers, J.W.H., Blais, B., Schouten, S. and Sinninghe Damsté, J.S. 2018. Molecular fossils from phytoplankton reveal secular PCO2 trend over the phanerozoic. *Science Advances* 4(11), pp. 1–8. doi: 10.1126/sciadv.aat4556.

Wong, W.W. and Sackett, W.M. 1978. Fractionation of stable carbon isotopes by marine phytoplankton. *Geochimica et Cosmochimica Acta* 42(12), pp. 1809–1815. doi: 10.1016/0016-7037(78)90236-3.

Yamaguchi, R. and Suga, T. 2019. Trend and Variability in Global Upper-Ocean Stratification Since the 1960s. *Journal of Geophysical Research: Oceans* 124(12), pp. 8933–8948. doi: 10.1029/2019JC015439.

Zalasiewicz, J. and Williams, M. 2009. A Geological History of Climate Change. In: Letcher, T. M. ed. *Climate Change: Observed Impacts on Planet Earth*. Elsevier, 2015, pp. 1–17. doi: 10.1016/B978-0-444-53301-2.00006-3.

Zalasiewicz, J., Williams, M., Haywood, A. and Ellis, M. 2011. The anthropocene: A new epoch of geological time? *Philosophical Transactions of the Royal Society A: Mathematical, Physical and Engineering Sciences* 369(1938), pp. 835–841. doi: 10.1098/rsta.2010.0339.

Zeebe, R.E. and Wolf-Gladrow, D.A. 2001. CO2 in seawater: equilibrium, kinetics, isotopes. Amsterdam, The Netherlands: Elsevier Science

Zhang, J., Quay, P.D. and Wilbur, D.O. 1995. Carbon isotope fractionation during gas-water exchange and dissolution of CO2. *Geochimica et Cosmochimica Acta* 59(1), pp. 107–114. doi: 10.1016/0016-7037(95)91550-D.

Zohary, T. et al. 2005. P-limited bacteria but N and P co-limited phytoplankton in the Eastern Mediterranean - A microcosm experiment. *Deep-Sea Research Part II: Topical Studies in Oceanography* 52(22–23), pp. 3011–3023. doi: 10.1016/j.dsr2.2005.08.011.